ACS OMEGA

Article

http://pubs.acs.org/journal/acsodf

Computational Modeling of Novel Bulk Materials for the Intermediate-Band Solar Cells

Murugesan Rasukkannu,*,† Dhayalan Velauthapillai,† and Ponniah Vajeeston‡

†Department of Computing, Mathematics and Physics, Western Norway University of Applied Sciences, Inndalsveien 28, 5063 Bergen, Norway

‡Department of Chemistry, Center for Materials Science and Nanotechnology, University of Oslo, P.O. Box 1033, Blindern, N-0315 Oslo, Norway

Supporting Information

ABSTRACT: Research communities have been studying materials with intermediate bands (IBs) in the middle of the band gap to produce efficient solar cells. Cells based on these materials could reach theoretical efficiencies up to 63.2%. In this comprehensive study, we investigate by means of accurate first-principle calculation the electronic band structure of 2100 novel compounds (bulk materials) to discover whether the IB is present in these materials. Our calculations are based on the density functional theory, using the generalized-gradient approximation for exchange and correlation terms and focusing on the band structure, the density of states, and the electron effective masses of the structures in the database. The IB structures are obtained by adding metallic or semimetallic atoms in the bulk material. By means of these calculations, we have clearly identified a number of compounds that may having high potential to be used as photovoltaic materials. We present here the numerical results for 17 novel IB materials, which could theoretically prove to be suitable for photovoltaic applications.

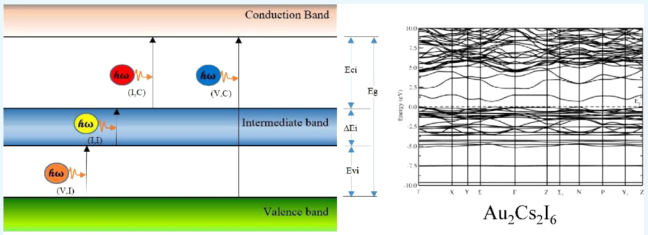

Research communities have been studying materials with intermediate bands in the middle of the bandgap to achieve efficient solar cells. Cells based on these materials could reach theoretical efficiencies up to 63.2%.

INTRODUCTION

Multi-band gap materials offer the possibility of increasing the efficiency of solar cells beyond the limit of traditional single-band gap solar-cell materials. Intermediate-band (IB) materials are characterized by the splitting of the main band gaps into two or more sub-band gaps by narrow IBs and have been the focus of recent studies.[1,2] In IB solar cells, an IB material is sandwiched between two ordinary p-type and n-type semiconductors and deed as discriminating contacts to the valence band (VB) and the conduction band (CB), respectively. In IB materials, an electron is promoted from the VB to the CB through the IB. Upon absorption of sub-band gap-energy photons, the electrons transit from VB to CB and later from IB to CB. It will add up to the transition of electrons from VB to CB through conventional VB-to-CB photon absorption.[1,2] By adopting a hypothesis similar to that of Shockley and Queisser,[3] it was shown in 1997[4] that balance-limiting efficiencies of 63.2% for IB solar cells and 41% for single-band gap solar cells can be achieved at a concentration of 46 050 suns at earth and sun temperatures of 300 and 6000 K, respectively.

The IB should be partially filled to permit the comparable rates for the low sub-band gap-energy photon absorption processes and should not overlap with either the VB or the CB to avoid fast transitions through thermalizations.[5] We can consider the IB solar cells as a combination of three cells. Cells representing VB-to-IB and IB-to-CB transitions can be regarded as two cells in series, and the VB-to-CB transition can represent a parallel cell. The cell will have a high tolerance to changes in the solar spectrum.[6]

In the mid-20th century, researchers[7−10] suggested the concept of creating intermediate levels in the middle of a forbidden band gap to increase the maximum photocurrent by doping the semiconductor with a large concentration of impurities. At an early stage, it was believed that these IBs would cause nonradiative recombination. It has been later shown that the nonradiative recombination can be suppressed by using a sufficiently high concentration of dopants.[10−13]

Two major approaches are considered in fabricating IB solar cells, namely, quantum-dot IBs (QDIBs) and bulk IB solar cells. By using quantum dots with different shapes and sizes, the IB levels can be tuned. The first QDIB was produced in 2004 on the basis of the InAs/GaAs QD material with an efficiency of 15.3%. Energy levels of the confined states in a quantum dot can be used as IB in QDIBs. However, there are many challenges with QDIBs as quantum dots are very small and do not absorb a significant amount of light. With an increasing number of QDs, the cell structure can be damaged, and strain will cause severe damages. At room temperature, the Shockley−Read−Hall recombination is a dominant mechanism that leads to low efficiency in QDIB solar cells due to deeper impurities.

Received: December 21, 2016
Accepted: March 31, 2017
Published: April 13, 2017

DOI: 10.1021/acsomega.6b00534
ACS Omega 2017, 2, 1454−1462

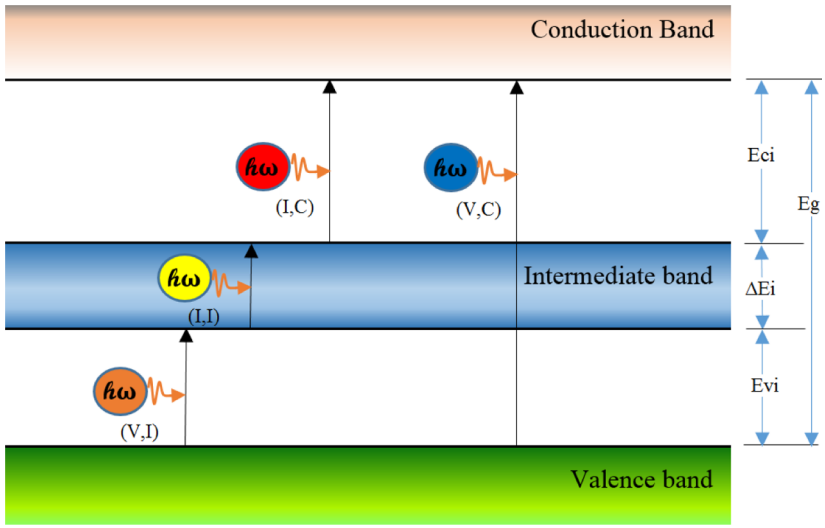

Figure 1. Band diagram of bulk IB solar cell; E_{vi}—energy gap between the top of the VB and the bottom of an IB, E_{ci}—energy gap between the top of the IB and the bottom of the CB, ΔE_i—width of the IB, E_g—total band gap between the top of the VB and the bottom of the CB. The electronic transitions (V, I), (I, I), (I, C), and (V, C) are also explained.

Table 1. Calculated Selected Narrow-Band Gap Semiconductors with IBs and Band Gap Type

serial no.	chemical formula	Pearson symbol	space group number	band gap (E_{vi})	band gap (E_{ci})	width of IB (ΔE_i)	total band gap (E_g)	band gap type
1.	K_6C_{60}	cI132	204	0.61	0.28	0.39	1.28	ID
2.	$Au_2Cs_2I_6$	tI20	139	0.64	1.01	0.7	2.35	ID
3.	Ag_2GeBaS_4	tI16	121	0.90	0.35	1.16	2.41	ID

Table 2. Wide-Band Gap 1 Semiconductors with IB Ranging from 2.62 to 3.15 eV

serial no.	chemical formula	Pearson symbol	space group number	band gap (E_{vi})	band gap (E_{ci})	width of IB (ΔE_i)	total band gap (E_g)	band gap type
1.	$CuAgPO_4$	oP56	61	1.27	0.61	0.74	2.62	DB
2.	Ag_2ZnSnS_4	tI16	121	0.47	0.57	1.66	2.70	DB
3.	$Au_2Cs_2Br_6$	tI20	139	0.67	1.23	0.81	2.71	DB
4.	Ag_3AsS_4	oP16	31	0.73	1.04	1.00	2.77	DB
5.	Ag_2KSbS_4	tI16	121	0.81	1.08	0.94	2.93	ID
6.	Na_3Se_4Sb	cI16	217	1.02	1.24	0.71	2.97	DB
7.	AgK_2SbS_4	oP32	118	1.52	1.03	0.47	2.97	DB
8.	$AsRb_3Se_4$	oP32	62	1.32	0.98	0.97	3.15	DB

Several research groups have produced QDIB solar cells,[14−22] and efficiencies over 18% have been reported by Blokhin et al.[20]

The second type of IB solar cells is based on bulk materials. The IB was detected through photoreflectance measurements in some bulk materials, and this formation was attributed to band anticrossing and heavily mismatched alloys.[23] The first of these bulk materials, ZnMnTeO, was developed by Walukiewicz and co-workers.[23] Later, numerous quantum-accurate calculations have been performed on VInS bulk material, characterized by an IB containing Fermi levels. Phillips and co-workers developed bulk IB solar cells using ZnTe doped with an oxygen atom and obtained higher efficiencies and short-circuit current than QDIB solar cells.[24,25] The band gap properties of bulk materials are widely studied, and the technologies are well verified by researchers.[5,26−33] However, the search for intermediate-band gap materials continues, to model high-efficiency IB solar cells. Figure 1 shows the band diagram of an IB solar cell with E_g, the total band gap between the top of the VB and the bottom of the CB. In the figure, E_{vi} is the energy gap between the top of the VB to the bottom of an IB, E_{ci} is the energy gap between the top of the IB to the bottom of the CB, and ΔE_i is the width of the IB. Furthermore, the electronic transitions of (V, I), (I, I), (I, C), and (V, C) are schematically depicted in the figure.

In the present work, we study 2100 structures with the aim of identifying ideal candidates for solar-cell materials. We employ density functional theory (DFT) calculations to verify the presence of an IB, isolated in the band gap of the semiconductor compounds of bulk material compounds with different substitutional impurities forming ternary alloys. The calculated band gap values are used to identify the most suitable compounds for solar-cell applications. We also present density of states (DOS) and effective mass calculations for the selected IB materials.

RESULTS AND DISCUSSION

The main focus of the present work is to find the potential IB materials from the selected 2100 compounds. Because of the very high computational cost, we mainly focused on the electronic structure, the DOS and effective mass calculations. The hybrid electronic structure and optical properties of the selected IB compounds are under investigation, and the results will be published in a forthcoming work. We employ the DFT method to elucidate the band structure arrangement of 2100

DOI: 10.1021/acsomega.6b00534
ACS Omega 2017, 2, 1454−1462

bulk materials, vital for the interaction of IB and could be potent solar cells with sufficient band gap. The DFT approaches to reveal the significant and computational features of the bulk materials and these features can be used as virtual screenings of band structures of the 2100 compounds to identify the novel IB compounds. From the first screening, we observed 312 compounds having an IB with the maximum of the VB at the Fermi level. Among these, 282 compounds were selected for further analysis and 30 compounds were found as heavy elements. After carrying out a detailed analysis, we found out that only 17 compounds among the starting 282 would be acceptable semiconductor materials for photovoltaic applications. The rest were found to be perfect insulators, with band gap values larger than 3.51 eV.[34] The electronic properties of these 17 compounds are presented in Tables 1−3. It is well known that the band gap (E_g) values of solids obtained from usual DFT calculations are systematically underestimated due to discontinuity in the exchange-correlation potential. Thus, the calculated E_g values are typically 30−50% smaller than those measured experimentally.[35] It is recognized that the theoretically calculated E_g for semiconductors and insulators are strongly dependent on the approximations used, particularly on the exchange and correlation terms of the potential. In the present work, because of the large number compounds involved in the screening process, we have used only generalized-gradient approximation. However, the overall structure is not going to change except the band gap value irrespective of the approximation.

Table 3. Calculated Effective Masses of Narrow-Band Gap Compounds; Light Holes (m^*_{lh}), Heavy Holes (m^*_{hh}), and Electrons (m^*_e)

serial no.	plane directions	compound	$m^*_{lh}\cdot m_e$	$m^*_{hh}\cdot m_e$	$m^*_e\cdot m_e$
1.	110	K_6C_{60}	0.092	0.164	0.216
2.	110	$Au_2Cs_2I_6$	0.096	0.265	0.095
3.	110	Ag_2GeBaS_4	0.059	0.114	0.021

We have chosen to divide the 17 compounds with IBs into three groups depending on the magnitude of their band gap values. The first group of three compounds is named as narrow-band gap semiconductors, which is characterized by band gaps varying from 1.2 to 2.5 eV. The second group of eight compounds is named wide-band gap 1 semiconductors, which includes materials with band gaps varying from 2.6 to 3.15 eV. Finally, the third group is named as wide-band gap 2 semiconductors. In this case, the band gap values vary from 3.15 to 3.5 eV. The band structures of these compounds are presented in Figures 2a−c, 3a−d, 4a−d, and 5a−f, and we calculate the total band gaps, band gaps E_{vi}, E_{ci}, and the widths of the IB (ΔE_i) bands for all of the compounds. The electronic structure properties of these compounds are presented in Tables 1, 2, and S1.

As presented in Table 1, narrow-band gap semiconductors K_6C_{60} (alkali fullerides), $Au_2Cs_2I_6$, and Ag_2GeBaS_4 had total indirect band gaps of 1.28, 2.35, and 2.41 eV, respectively.

From Figure 2a, the calculated values for K_6C_{60} are: The total indirect band gap is 1.28 eV, band gaps E_{vi} and E_{ci} are 0.61 and 0.28 eV, respectively, and the width of the IB is 0.39 eV. The band gap of 1.28 eV makes an optimal compound for the PV applications as their light responses are in the infrared region. Also, the IB will help the material to absorb additional photons with lower energy. It should be noted that K_6C_{60} is already known as a semiconductor and the nature of the band structure is not well explained about the IB. However, they explained that the electronic structure of crystalline K_6C_{60} is indirect band gap of 0.48 eV.[36] The DOS around the VB maximum is very similar to that of the isolated C_{60} molecule, and the K atoms are almost completely ionized.[36]

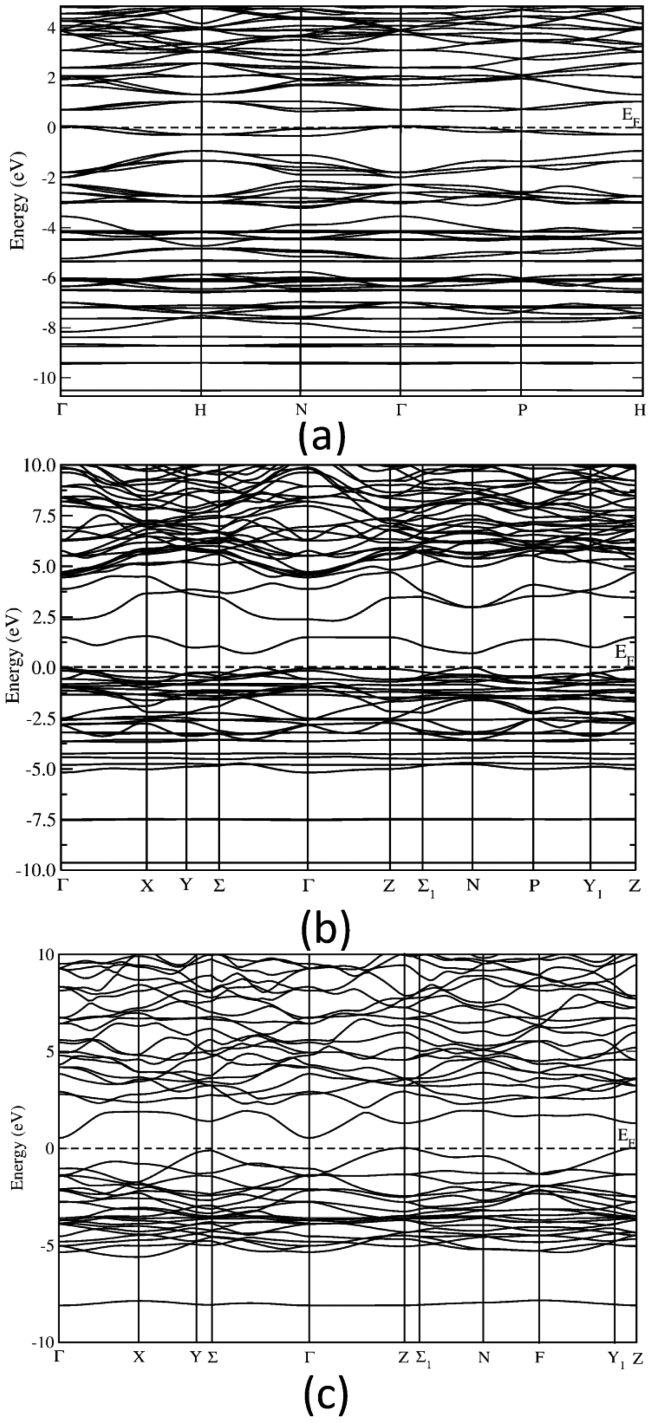

Figure 2. Calculated electronic band structures of (a) K_6C_{60}, (b) $Au_2Cs_2I_6$, (c) and Ag_2GeBaS_4. The Fermi level is set to zero.

Similarly, from Figure 2b, the calculated values for $Au_2Cs_2I_6$ are as follows: The total indirect band gap is 2.35 eV, band gaps E_{vi} and E_{ci} are 0.64 and 1.01 eV, respectively, and the width of the IB, ΔE_i is 0.70 eV. The band gap of 2.35 eV for $Au_2Cs_2I_6$ shows that the material has its response to light in the visible

DOI: 10.1021/acsomega.6b00534
ACS Omega 2017, 2, 1454−1462

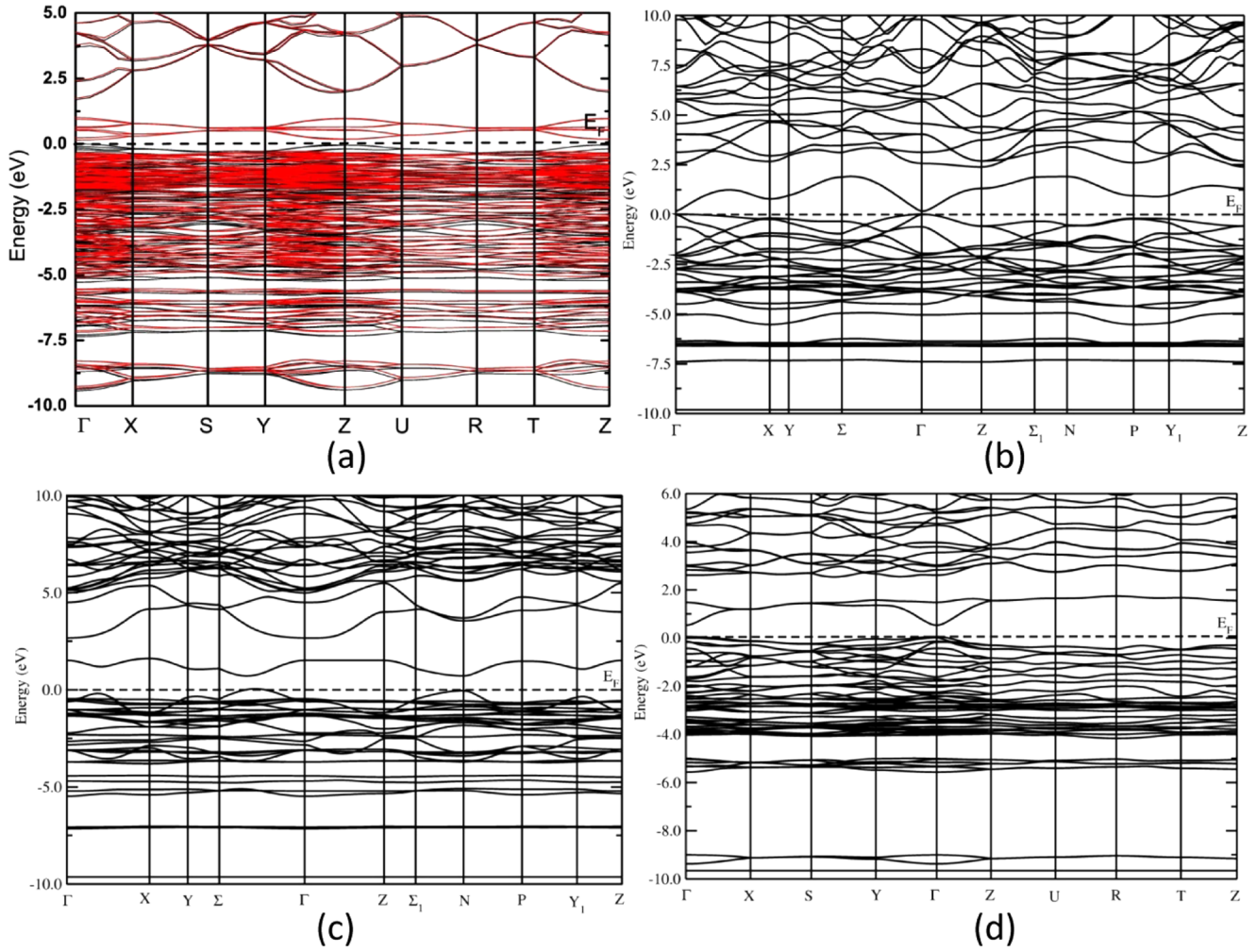

Figure 3. Calculated electronic band structures of (a) $CuAgPO_4$ (up and down spin bands; up—black, down—red), (b) Ag_2ZnSnS_4, (c) $Au_2Cs_2Br_6$, and (d) Ag_3AsS_4. The Fermi level is set to zero.

region. For $Au_2Cs_2I_6$, the IB region has the optimal thickness to balance the absorption rate and recombination rate.[37] In Figure 2b, $Au_2Cs_2I_6$ has a broad band dispersion of IB, enough to produce an optical depth for subgap light, ensuring the compound to absorb subgap light so that it can be considered as a potential PV material.[37]

From Figure 2c, the calculated values for Ag_2GeBaS_4 are: The total indirect band gap is 2.41 eV, band gaps E_{vi} and E_{ci} are 0.90 and 0.35 eV, respectively, and the width of the IB is 1.16 eV. The band gap of 2.35 eV for Ag_2GeBaS_4 shows that the material has its response to light in the visible region. Here, we observe that the width of the IB, ΔE_i, in Ag_2GeBaS_4 is much higher than E_{ci} and E_{vi}. Because of the broadness of the IB, photons can also be absorbed by the electrons from lower-energy states of the IB to excite to higher-energy states of IB. When the IB broadens, the absorption of photons for the transition of electrons from the VB to lower-energy states of IB as well as from the higher-energy states of IB to CB will be reduced. These effects will lead to lower efficiencies of the solar cell based on Ag_2GeBaS_4. It has been shown that the efficiency limit for an IB solar cell is reduced from higher to lower efficiencies if the width is infinitesimally significant.[38] It is important to note that all of these three materials, K_6C_{60}, $Au_2Cs_2I_6$, and Ag_2GeBaS_4, present indirect band gaps.

As presented in Table 2, the wide-band gap semiconductors $CuAgPO_4$, Ag_2ZnSnS_4, $Au_2Cs_2Br_6$, Ag_3AsS_4, Ag_2KSbS_4, Na_3Se_4Sb, AgK_2SbS_4, and $AsRb_3Se_4$ had the total band gaps of 2.62, 2.70, 2.71, 2.77, 2.93, 2.97, 2.97, and 3.15 eV, respectively. Figures 3a–d and 4a–d show the calculated band structures of $CuAgPO_4$, Ag_2ZnSnS_4, $Au_2Cs_2Br_6$, Ag_3AsS_4, Ag_2KSbS_4, Na_3Se_4Sb, AgK_2SbS_4, and $AsRb_3Se_4$ with IB, respectively. The calculated values of E_{vi}, E_{ci}, and ΔE_i, and the total band gaps are presented in Table 2. The band gap type of the above eight compounds is direct band gap except for Ag_2KSbS_4 (indirect band gap). From Figure 2c, the calculated values for Ag_2ZnSnS_4 are: The total direct band gap is 2.70 eV, band gaps E_{vi} and E_{ci} are 0.47 and 0.57 eV, respectively, and the width of the IB is 1.66 eV. The band gap of 2.70 eV for Ag_2ZnSnS_4 shows that the material has its response to light in the visible region. Here, we observe that the width of the IB, ΔE_i, in Ag_2ZnSnS_4 is much higher than E_{ci} and E_{vi}. The increase in the IB width leads to a decrease in efficiency; however, it is still significantly higher than that of a single-band gap solar cell.[39] The band gaps associated with optimum efficiencies are constant for all IB solar cells when the IB width exceeds 2 eV.[39] Because of the display of the small amount of data, we added the remaining six compounds in the Supporting Information.

In general, the electrochemical potentials of the electrons in the different bands are close to the edges of the bands. The

DOI: 10.1021/acsomega.6b00534
ACS Omega 2017, 2, 1454–1462

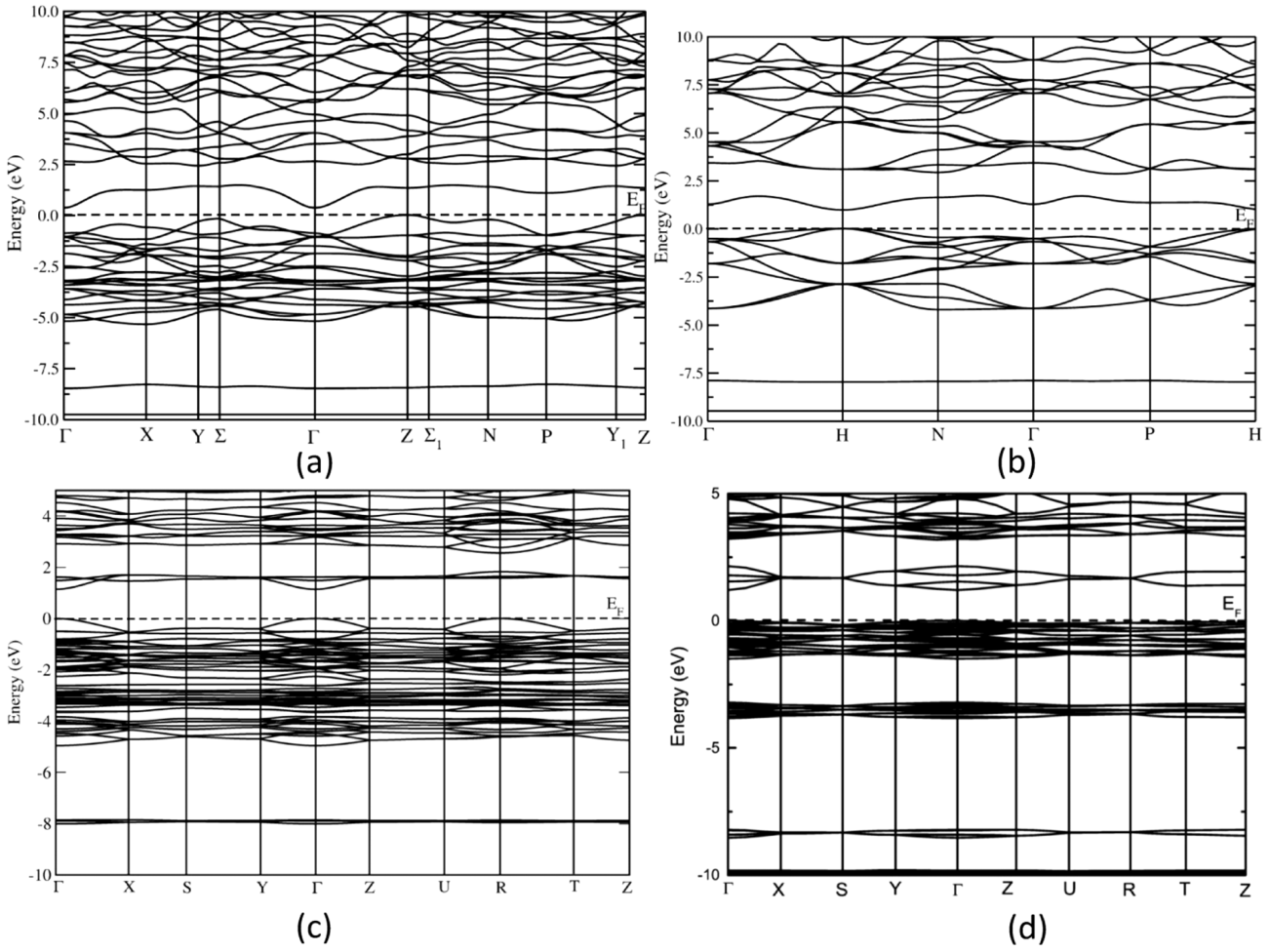

Figure 4. Calculated electronic band structures of (a) Ag_2KSbS_4, (b) Na_3Se_4Sb, (c) AgK_2SbS_4, and (d) $AsRb_3Se_4$. The Fermi level is set to zero.

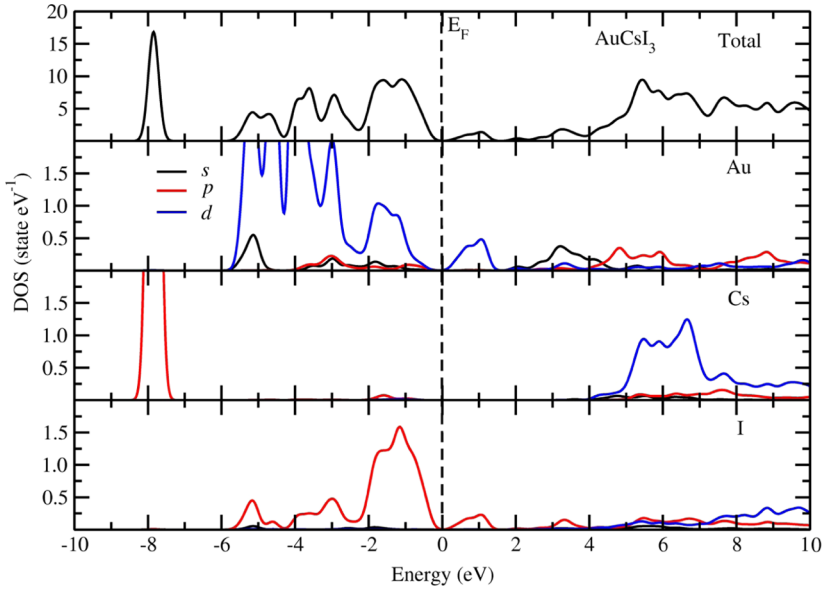

Figure 5. Total and site-projected DOS of $Au_2Cs_2I_6$. The Fermi level is set to zero and marked by a vertical dotted line.

open-circuit voltage of any solar cell is the difference between the CB minimum at the electrode in contact with the n-type side and the VB maximum at the electrode in contact with the p-type side. Thus, the maximum photovoltage of IB solar cells on the materials presented in Tables 1 and S1 is limited to 2.41 and 3.51 eV, respectively. Ag_2GeBaS_4 is still capable of absorbing energy photons above 0.28 eV in Table 1 and Ag_6SiSO_8 of 0.47 eV in Table 2. IB solar cells can deliver a maximum photovoltage by absorbing two sub-band gap

DOI: 10.1021/acsomega.6b00534
ACS Omega 2017, 2, 1454−1462

photons to produce one high-energy electron; the laws of thermodynamics would be violated if this were not the case.[1]

All of the 17 semiconductor compounds presented in this work have properties that make them suitable for PV applications; we show here the DOS analysis for three compounds, namely, $Au_2Cs_2I_6$, Ag_2GeBaS_4, and Ag_2ZnSnS_4. The band gaps of 1.28 and 2.41 eV, respectively, make $Au_2Cs_2I_6$ and Ag_2GeBaS_4 optimal PV materials. Solar cells based on Ag_2ZnSnS_4 materials are interesting as a high efficiency gain for these types of cells has been recently observed.[40] There are also reports on the possibilities to integrate Ag_2ZnSnS_4 in the Cu-based solar cells as an additional absorption layer.[40] The total DOS of $Au_2Cs_2I_6$ in Figure 5 shows that the IB is formed in the energy region between 0.64 and 1.34 eV. The IB composed of I 2p are described by the projected density of states (PDOS), as shown in Figure 5. Figure 6 shows that the IB is formed in the

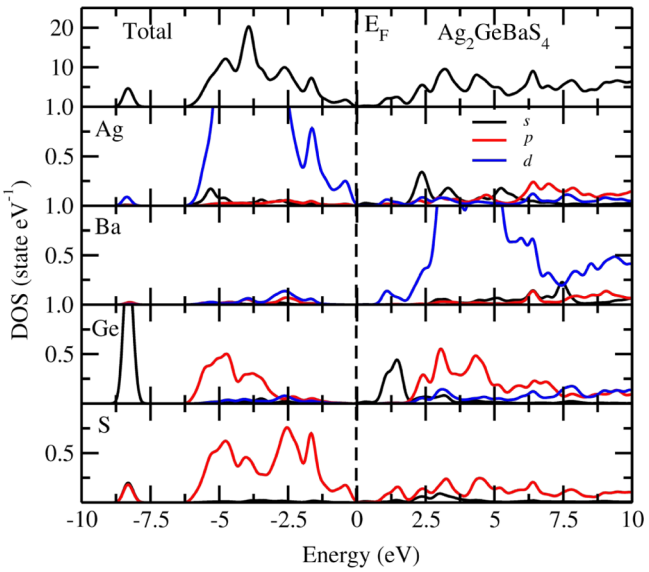

Figure 6. Total and site PDOS of Ag_2GeBaS_4. The Fermi level is set to zero and marked by a vertical dotted line.

energy region between 0.90 and 2.06 eV of the total DOS of Ag_2GeBaS_4. We have also plotted the PDOS at the IB mainly composed of the S 2p band and the Ge 4s band as well as the smaller mixing of the Ba 4d band. For Ag_2ZnSnS_4, the IB is formed in the energy region between 0.47 and 2.13 eV, and the electron density, as shown in Figure 7 better describes the states. The PDOS of Ag_2ZnSnS_4 at the IB mainly composed of the Sn 5s band and the S 2p band is shown in Figure 7. The Ag_2ZnSnS_4 has an energy gap of 2.62 eV. We found the excellent IB peaks between CB and VB in the three materials, namely, $Au_2Cs_2I_6$, Ag_2GeBaS_4, and Ag_2ZnSnS_4. We observed that the p and s states play a vital role in the band structure for the applicability of semiconductor for PV applications.

In Figures 5−7, broadening of IB indicates a highly parabolic dispersion relationship that induces lower values for the DOS.[41] From Tables 3 and 4, the electron effective masses of $Au_2Cs_2I_6$, Ag_2GeBaS_4, and Ag_2ZnSnS_4 are $0.095m_e$, $0.021m_e$, and $0.025m_e$, respectively. Lower values for the electron effective mass are as expected because the effective mass is directly related to the values of DOS. In addition, the IB region has the optimal thickness to balance the absorption rate and the recombination rate.[37] We may expect the effective IBSC to have IB thickness enough to ensure these materials to absorb sufficient subgap

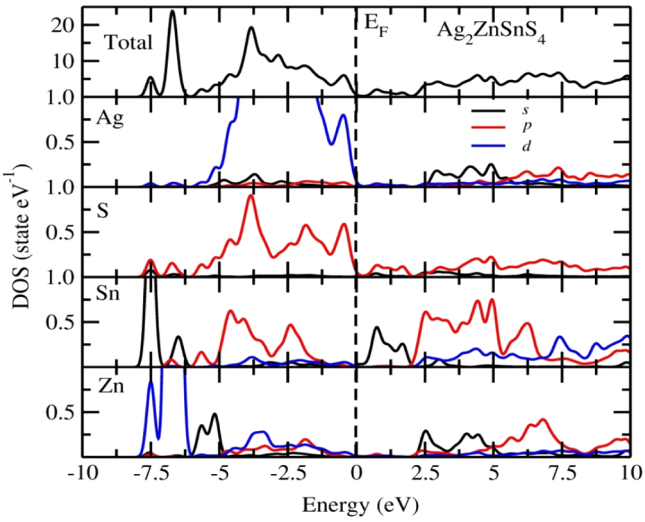

Figure 7. Total and site PDOS of Ag_2ZnSnS_4. The Fermi level is set to zero and marked by a vertical dotted line.

Table 4. Effective Mass of Wide-Band Gap IB Compounds

serial no.	plane directions	compound	$m^*_{lh}\cdot m_e$	$m^*_{hh}\cdot m_e$	$m^*_e\cdot m_e$
1.	100	$CuAgPO_4$	3.875	4.969	14.229
2.	110	Ag_2ZnSnS_4	0.033	0.237	0.025
3.	110	$Au_2Cs_2Br_6$	0.870	1.810	0.806
4.	100	Ag_3AsS_4	0.200	0.234	0.012
5.	110	Ag_2KSbS_4	0.125	0.526	0.034
6.	110	Na_3Se_4Sb	0.377	0.381	0.085
7.	100	AgK_2SbS_4	1.524	12.025	1.007
8.	100	$AsRb_3Se_4$	6.213	84.330	2.595
9.	100	$AsCs_3Se_4$	8.213	24.794	3.561
10.	110	Al_2HgSe_4	0.070	0.255	0.021
11.	110	$PdPbF_4$	0.391	0.592	0.094
12.	100	$C_2Te_2F_4$	3.293	5.165	7.659
13.	100	$AlMoVO_7$	1.680	2.756	1.959
14.	110	Ag_6SiSO_8	0.145	2.634	0.053

light. We conclude that the conversion efficiency of bulk IBSC strongly depends not only on the band gap but also on the position and thickness of IB and DOS.[37,41]

EFFECTIVE MASS CALCULATION

The calculation of the effective mass is important for a detailed study of energy levels in solar devices. The conductivity effective masses of electrons and holes affect the mobility, electrical resistivity, and free-carrier optical response of photovoltaic applications.[42] To investigate the electron/hole conduction properties of the identified IB materials, we have computed the electron/hole effective mass at the VB/CB. For an excellent IB, a low effective mass corresponds to a high mobility of the electrons/holes at the VB/CB and consequently high conductivity. For the EM calculation, we have employed the effective mass calculator (EMC).[43] EMC implements the calculation of the effective masses at the bands extreme using the finite difference method (FDM) (not the band-fitting method). The effective mass (m^*) of charge carriers is defined as[43]

$$\left(\frac{1}{m^*}\right)_{ij} = \frac{1}{\hbar^2}\frac{\partial^2 E_n(\vec{k})}{\partial k_i k_j}, \quad i, j = x, y, z \tag{1}$$

DOI: 10.1021/acsomega.6b00534
ACS Omega 2017, 2, 1454−1462

where x, y, and z are the directions in the reciprocal Cartesian space $(2\pi/A)$, $E_n(k)$ is the dispersion relation for the nth electronic band, and indices i and j denote reciprocal components. The explicit form of the symmetric tensor in the right-hand side of eq 1 is[43]

$$\frac{d^2E}{dk^2} = \begin{pmatrix} \frac{d^2E}{dk_x^2} & \frac{d^2E}{dk_x\,dk_y} & \frac{d^2E}{dk_x\,dk_z} \\ \frac{d^2E}{dk_x\,dk_y} & \frac{d^2E}{dk_y^2} & \frac{d^2E}{dk_y\,dk_z} \\ \frac{d^2E}{dk_x\,dk_z} & \frac{d^2E}{dk_y\,dk_z} & \frac{d^2E}{dk_z^2} \end{pmatrix} \quad (2)$$

The effective mass components are the inverse of the eigenvalues of eq 2, and the principal directions correspond to the eigenvectors.[43]

To better understand the effective mass of semiconductors, it is not possible to fit the band to the quadratic polynomial. In this case, the results from the parabolic fitting can be reproduced with the FDM.[43] The FDM employed to solve the effective mass approximation equations because the spurious solutions can be included in the formalism, and the FDM can be solved by the hard equation having a high degree of polynomial.[44] This approach is quite reliable, and it was successfully applied for several classes of materials in the literature.[43] We present the effective masses of 14 compounds in Tables 3 and 4. The effective mass of an electron was computed from the minimum of the CB; the effective mass of the heavy hole was computed from the maximum of the first VB curvature, whereas the second VB curvature was used for the light hole. In the case of materials presented in Tables 3 and 4, the PBE functional predicts the effective masses of the light hole, heavy hole, and electron, which are parabolic-fitted values with a step size of 0.05 (1/bohr). The three narrow-band gap compounds, K_6C_{60}, $Au_2Cs_2I_6$, and Ag_2GeBaS_4, have low effective masses, as presented in Table 3.

The thirteen wide-band gap compounds in Table 4 have effective masses of electron lower than those of light holes and heavy holes except for $CuAgPO_4$. The effective masses of electron of photovoltaic materials silicon (Si), germanium (Ge), and gallium arsenide (GaAs) are $0.26m_e$, $0.067m_e$, and $0.12m_e$, respectively.[45,46] The above three photovoltaic materials are single-band gap materials. It is well known that the band gaps of Si, Ge, and GaAs are 1.12, 0.66, and 1.424 eV, respectively. The maximum energy conversion of silicon and GaAs solar cells can reach 30% efficiency.[48] We can use germanium as the doping material in silicon solar cells because of its low band gap. We noticed that the effective masses of the electron for the silicon and GaAs are low.[45] From our results, we observed that the effective masses of electron for K_6C_{60}, $Au_2Cs_2I_6$, and Ag_2GeBaS_4 are $0.216m_e$, $0.095m_e$, and $0.021m_e$, respectively.

From Table 4, we noted that the effective masses of electron for Ag_2ZnSnS_4, $Au_2Cs_2Br_6$, Ag_3AsS_4, Ag_2KSbS_4, Na_3Se_4Sb, Al_2HgSe_4, $PdPbF_4$, Ag_6SiSO_8 are $0.025m_e$, $0.806m_e$, $0.012m_e$, $0.034m_e$, $0.085m_e$, $0.021m_e$, $0.094m_e$, and $0.053m_e$, respectively. Hence, the effective masses of electron of our narrow-band gap and wide-band gap materials are approximately equal to those of the photovoltaic materials. From Table 4, the effective mass of an electron is $0.025m_e$ for Ag_2ZnSnS_4 in [110] plane direction. We observed from Jing et al. that the effective mass of an electron is $0.16m_e$ for Ag_2ZnSnS_4 in [100] plane direction.[42] Hence, we found a lower effective mass in [110] direction than in [100] direction. These effective masses are better described by the band structures of the most curved parabolic band, as shown in Figures 3−5. Because of the effective masses for the presented materials, in this article, the electron mobility from VB to CB will be higher and the recombination effect will be lower.

CONCLUSIONS

We have carried out a comprehensive study of the electronic band structures of 2100 new bulk compounds using first-principle calculations with the DFT. Among these compounds, we have found that only 17 compounds have IBs. These compounds could be potentially used as photovoltaic materials based on the detailed studies of band structure, the DOS and effective mass calculations. Our effective mass calculations show that these compounds have high electron/hole conduction properties, which make them suitable for PV applications. Although we have studied 2100 new compounds from the ICSD database, our study clearly demonstrates the possibility of having more IB materials from the list of currently known compounds from the database. Thus, we are in the process of investigating more IB-compounds and results of the detailed analysis will be published in a forthcoming article.

COMPUTATIONAL DETAILS

Total energies have been calculated by the projected augmented plane-wave (PAW) implementation of the Vienna ab initio simulation package.[47] Ground-state geometries were determined by minimizing stresses and the Hellman−Feynman forces using the conjugate-gradient algorithm with a force convergence threshold if 10^{-3} eV Å^{-1}. Brillouin-zone integration was performed using the Monkhorst−Pack k-meshes with a Gaussian broadening of 0.1 eV. A 600 eV kinetic energy cutoff was used for the plane-wave expansion. All of these calculations usually set to use approximately the same density of k-points in the reciprocal space for all structures. Because a large variety of structures was considered in this study, both metallic and insulating, we ensured that the k-points mesh was dense enough to determine the total energy with meV/atom accuracy. All structures containing transition elements are treated using the spin-polarized approach. In some cases, the starting magnetization vanished as self-consistency was reached. For all of these computations, the starting structures were directly taken from the ICSD database and input parameters, and file generation was done automatically by locally developed code "Tool". For the calculation of band structure, the k-point files were generated again with the help of locally developed code "KPATH". The information about the high symmetric points of the k-vector in the Brillouin zone was taken from the Bilbao Crystallographic Server.[48−50] All of the calculated electronic structures of the studied systems are documented in the DFTBD database. For the transition metals, we have used exchange-correlation functional with the Hubbard parameter correction (GGA+U), following the rotationally invariant form. The full details about the computed U and J values are presented in the DFTBD database website.[51−54]

DOI: 10.1021/acsomega.6b00534
ACS Omega 2017, 2, 1454−1462

■ ASSOCIATED CONTENT

Supporting Information

The Supporting Information is available free of charge on the ACS Publications website at DOI: 10.1021/acsomega.6b00534.

Tables, list of computed compounds and figures (PDF)

■ AUTHOR INFORMATION

Corresponding Author

*E-mail: rmu@hvl.no.

ORCID

Murugesan Rasukkannu: 0000-0002-2167-3242

Notes

The authors declare no competing financial interest.

■ ACKNOWLEDGMENTS

The authors gratefully acknowledge the Bergen University College for financially supporting M.R. P.V. and D.V. acknowledge the NOTUR computing facilities of project. numbers NN2867K and NN2875K, which have been used to conduct the calculations presented in this article, and further acknowledge Dr.Vishnu for fruitful discussions.

■ REFERENCES

(1) Luque, A.; Marti, A.; Stanley, C. Understanding Intermediate-Band Solar Cells. *Nat. Photonics* **2012**, *6*, 146−152.

(2) Luque, A.; Marti, A. A metallic intermediate band high efficiency solar cell. *Prog. Photovoltaics* **2001**, *9*, 73−86.

(3) Shockley, W.; Queisser, H. J. Detailed balance limit of efficiency of p-n junction solar cells. *J. Appl. Phys.* **1961**, *32*, 510−519.

(4) Luque, A.; Martí, A. Increasing the efficiency of ideal solar cells by photon induced transitions at intermediate levels. *Phys. Rev. Lett.* **1997**, *78*, 5014.

(5) Palacios, P.; Aguilera, I.; Sánchez, K.; Conesa, J.; Wahnón, P. Transition-metal-substituted indium thiospinels as novel intermediate-band materials: prediction and understanding of their electronic properties. *Phys. Rev. Lett.* **2008**, *101*, No. 046403.

(6) Green, M. A. Multiple band and impurity photovoltaic solar cells: general theory and comparison to tandem cells. *Prog. Photovoltaics* **2001**, *9*, 137−144.

(7) Shockley, W.; Read, W., Jr. Statistics of the recombinations of holes and electrons. *Phys. Rev.* **1952**, *87*, 835−842.

(8) Hall, R. N. Electron-hole recombination in germanium. *Phys. Rev.* **1952**, *87*, 387.

(9) Lang, D.; Henry, C. Nonradiative recombination at deep levels in GaAs and GaP by Lattice-Relaxation Multiphonon Emission. *Phys. Rev. Lett.* **1975**, *35*, 1525.

(10) Wolf, M. Limitations and possibilities for improvement of photovoltaic solar energy converters: part I: considerations for earth's surface operation. *Proc. IRE* **1960**, *48*, 1246−1263.

(11) Ekins-Daukes, N.; Honsberg, C.; Yamaguchi, M. In *Signature of Intermediate Band Materials from Luminescence Measurements*, Proceedings of the 31st IEEE Photovoltaic Specialists Conference, 2005; IEEE, 2005; pp 49−54.

(12) Strandberg, R.; Reenaas, T. W. Photofilling of intermediate bands. *J. Appl. Phys.* **2009**, *105*, No. 124512.

(13) Levy, M. Y.; Honsberg, C. Solar cell with an intermediate band of finite width. *Phys. Rev. B* **2008**, *78*, No. 165122.

(14) Hubbard, S.; Cress, C.; Bailey, C.; Raffaelle, R.; Bailey, S.; Wilt, D. Effect of strain compensation on quantum dot enhanced GaAs solar cells. *Appl. Phys. Lett.* **2008**, *92*, No. 123512.

(15) Oshima, R.; Takata, A.; Okada, Y. Strain-compensated InAs/GaNAs quantum dots for use in high-efficiency solar cells. *Appl. Phys. Lett.* **2008**, *93*, No. 083111.

(16) Kechiantz, A.; Sun, K.; Kechiyants, H.; Kocharyan, L. Self-ordered Ge/Si quantum dot intermediate band photovoltaic solar cells. *ISJAEE* **2005**, *12*, 85−87.

(17) Laghumavarapu, R.; El-Emawy, M.; Nuntawong, N.; Moscho, A.; Lester, L.; Huffaker, D. Improved device performance of InAs/GaAs quantum dot solar cells with GaP strain compensation layers. *Appl. Phys. Lett.* **2007**, *91*, 243115.

(18) Popescu, V.; Bester, G.; Hanna, M. C.; Norman, A. G.; Zunger, A. Theoretical and experimental examination of the intermediate-band concept for strain-balanced (In, Ga) As/Ga (As, P) quantum dot solar cells. *Phys. Rev. B* **2008**, *78*, No. 205321.

(19) Bailey, C. G.; Forbes, D. V.; Raffaelle, R. P.; Hubbard, S. M. Near 1 V open circuit voltage InAs/GaAs quantum dot solar cells. *Appl. Phys. Lett.* **2011**, *98*, No. 163105.

(20) Blokhin, S.; Sakharov, A.; Nadtochy, A.; Pauysov, A.; Maximov, M.; Ledentsov, N.; Kovsh, A.; Mikhrin, S.; Lantratov, V.; Mintairov, S.; et al. AlGaAs/GaAs photovoltaic cells with an array of InGaAs QDs. *Semiconductors* **2009**, *43*, 514−518.

(21) Guimard, D.; Morihara, R.; Bordel, D.; Tanabe, K.; Wakayama, Y.; Nishioka, M.; Arakawa, Y. Fabrication of InAs/GaAs quantum dot solar cells with enhanced photocurrent and without degradation of open circuit voltage. *Appl. Phys. Lett.* **2010**, *96*, No. 203507.

(22) Zhou, D.; Sharma, G.; Thomassen, S.; Reenaas, T.; Fimland, B. Optimization towards high density quantum dots for intermediate band solar cells grown by molecular beam epitaxy. *Appl. Phys. Lett.* **2010**, *96*, No. 061913.

(23) Walukiewicz, W.; Shan, W.; Yu, K.; Ager, J., III; Haller, E.; Miotkowski, I.; Seong, M.; Alawadhi, H.; Ramdas, A. Interaction of localized electronic states with the conduction band: Band anticrossing in II−VI semiconductor ternaries. *Phys. Rev. Lett.* **2000**, *85*, 1552.

(24) Wang, W.; Lin, A. S.; Phillips, J. D. Intermediate-band photovoltaic solar cell based on ZnTe: O. *Appl. Phys. Lett.* **2009**, *95*, No. 011103.

(25) Wang, W.; Lin, A. S.; Phillips, J. D.; Metzger, W. K. Generation and recombination rates at ZnTe: O intermediate band states. *Appl. Phys. Lett.* **2009**, *95*, No. 261107.

(26) Antolín, E.; Martí, A.; Olea, J.; Pastor, D.; González-Díaz, G.; Mártil, I.; Luque, A. Lifetime recovery in ultrahighly titanium-doped silicon for the implementation of an intermediate band material. *Appl. Phys. Lett.* **2009**, *94*, No. 042115.

(27) Wahnón, P.; Tablero, C. Ab initio electronic structure calculations for metallic intermediate band formation in photovoltaic materials. *Phys. Rev. B* **2002**, *65*, No. 165115.

(28) Ling, C.; Zhou, L. Q.; Banerjee, D.; Jia, H. Band structures of ZnTe: O alloys with isolated oxygen and with clustered oxygen impurities. *J. Alloys Compd.* **2014**, *584*, 289−294.

(29) Strandberg, R. Evaluation of a selection of intermediate band materials based on their absorption coefficients. *IEEE J. Photovoltaics* **2013**, *3*, 997−1003.

(30) Aguilera, I.; Palacios, P.; Sánchez, K.; Wahnón, P. Theoretical optoelectronic analysis of $MgIn_2S_4$ and $CdIn_2S_4$ thiospinels: effect of transition-metal substitution in intermediate-band formation. *Phys. Rev. B* **2010**, *81*, No. 075206.

(31) Kong-Ping, W.; Shu-Lin, G.; Jian-Dong, Y.; Kun, T.; Shun-Ming, Z.; Meng-Ran, Z.; You-Rui, H.; Rong, Z.; You-Dou, Z. Theoretical optoelectronic analysis of intermediate-band photovoltaic material based on ZnY1 − xOx (Y = S, Se, Te) semiconductors by first-principles calculations. *Chin. Phys. B* **2013**, *22*, No. 107103.

(32) Palacios, P.; Wahnón, P.; Pizzinato, S.; Conesa, J. C. Energetics of formation of $TiGa_3As_4$ and $TiGa_3P_4$ intermediate band materials. *J. Chem. Phys.* **2006**, *124*, No. 014711.

(33) Sánchez, K.; Aguilera, I.; Palacios, P.; Wahnón, P. Assessment through first-principles calculations of an intermediate-band photovoltaic material based on Ti-implanted silicon: Interstitial versus substitutional origin. *Phys. Rev. B* **2009**, *79*, No. 165203.

(34) Huang, F.-W.; Sheu, J.-K.; Lee, M.-L.; Tu, S.-J.; Lai, W.-C.; Tsai, W.-C.; Chang, W.-H. Linear photon up-conversion of 450 meV in InGaN/GaN multiple quantum wells via Mn-doped GaN intermediate band photodetection. *Opt. Express* **2011**, *19*, A1211−A1218.

DOI: 10.1021/acsomega.6b00534
ACS Omega 2017, 2, 1454−1462

(35) Lundqvist, S.; March, N. H. *Theory of the Inhomogeneous Electron Gas*; Springer US, 1983; pp 309−389.
(36) Erwin, S. C.; Pederson, M. R. Electronic structure of crystalline K_6C_{60}. *Phys. Rev. Lett.* **1991**, *67*, 1610.
(37) Sullivan, J. T.; Simmons, C. B.; Buonassisi, T.; Krich, J. J. Targeted search for effective intermediate band solar cell materials. *IEEE J. Photovoltaics* **2015**, *5*, 212−218.
(38) Levy, M. Y.; Honsberg, C. Solar cell with an intermediate band of finite width. *Phys. Rev. B* **2008**, *78*, No. 165122.
(39) Levy, M. Y.; Honsberg, C. Intraband absorption in solar cells with an intermediate band. *J. Appl. Phys.* **2008**, *104*, No. 113103.
(40) Jing, T.; Dai, Y.; Ma, X.; Wei, W.; Huang, B. Electronic Structure and Photocatalytic Water-Splitting Properties of $Ag_2ZnSn(S1-x\ Se\ x)_4$. *J. Phys. Chem. C* **2015**, *119*, 27900−27908.
(41) Okada, Y.; Ekins-Daukes, N.; Kita, T.; Tamaki, R.; Yoshida, M.; Pusch, A.; Hess, O.; Phillips, C.; Farrell, D.; Yoshida, K.; et al. Intermediate band solar cells: Recent progress and future directions. *Appl. Phys. Rev.* **2015**, *2*, No. 021302.
(42) Riffe, D. M. Temperature dependence of silicon carrier effective masses with application to femtosecond reflectivity measurements. *J. Opt. Soc. Am. B* **2002**, *19*, 1092−1100.
(43) Fonari, A.; Sutton, C. Validation of the Effective Masses Calculated Using Finite Difference Method on a Five-Point Stencil for Inorganic and Organic Semiconductors. 2013, arXiv:condensed matter/1302.4996. arXiv.org e-Print archive. https://arxiv.org/abs/1302.4996.
(44) Cartoixa, X.; Ting, D.-Y.; McGill, T. Numerical spurious solutions in the effective mass approximation. *J. Appl. Phys.* **2003**, *93*, 3974−3981.
(45) Van Zeghbroeck, B. *Principles of Semiconductor Devices*; Colarado University, 2004.
(46) Green, M. A.; Emery, K.; Hishikawa, Y.; Warta, W.; Dunlop, E. D. Solar cell efficiency Tables (Version 45). *Prog. Photovoltaics* **2015**, *23*, 1−9.
(47) Kresse, G.; Furthmüller, J. Efficient iterative schemes for ab initio total-energy calculations using a plane-wave basis set. *Phys. Rev. B* **1996**, *54*, 11169−11186.
(48) Aroyo, M.; Perez-Mato, J.; Orobengoa, D.; Tasci, E.; De La Flor, G.; Kirov, A. Crystallography online: Bilbao crystallographic server. *Bulg. Chem. Commun.* **2011**, *43*, 183−197.
(49) Aroyo, M. I.; Perez-Mato, J. M.; Capillas, C.; Kroumova, E.; Ivantchev, S.; Madariaga, G.; Kirov, A.; Wondratschek, H. Bilbao Crystallographic Server: I. Databases and crystallographic computing programs. *Z. Kristallogr. - Cryst. Mater.* **2006**, *221*, 15−27.
(50) Aroyo, M. I.; Kirov, A.; Capillas, C.; Perez-Mato, J.; Wondratschek, H. Bilbao Crystallographic Server. II. Representations of crystallographic point groups and space groups. *Acta Crystallogr., Sect. A: Found. Crystallogr.* **2006**, *62*, 115−128.
(51) Dudarev, S.; Botton, G.; Savrasov, S. Y.; Szotek, Z.; Temmerman, W.; Sutton, A. Electronic Structure and Elastic Properties of Strongly Correlated Metal Oxides from First Principles: LSDA + U, SIC-LSDA and EELS Study of UO_2 and NiO. *Phys. Status Solidi A* **1998**, *166*, 429−443.
(52) Kresse, G.; Furthmüller, J. Efficiency of ab-initio total energy calculations for metals and semiconductors using a plane-wave basis set. *Comput. Mater. Sci.* **1996**, *6*, 15−50.
(53) Liechtenstein, A.; Anisimov, V.; Zaanen, J. Density-functional theory and strong interactions: Orbital ordering in Mott-Hubbard insulators. *Phys. Rev. B: Condens. Matter Mater. Phys.* **1995**, *52*, No. R5467.
(54) Perdew, J. P.; Burke, K.; Ernzerhof, M. Generalized gradient approximation made simple. *Phys. Rev. Lett.* **1996**, *77*, 3865.

DOI: 10.1021/acsomega.6b00534
ACS Omega 2017, 2, 1454−1462

Computational Modeling of New bulk materials for the Intermediate Band Solar cells

Murugesan Rasukkannu[1], Dhayalan Velauthapillai[1], Ponniah Vajeeston[2]
[1]*Western Norway University of Applied Sciences, Department of Computing, Mathematics and Physics, Inndalsveien 28, Box 5063, Bergen, Norway*

[2]*Center for Materials Science and Nanotechnology, Department of Chemistry, University of Oslo, Box 1033 Blindern N-0315, Oslo, Norway*

Supporting information, tables, list of computed compounds and figures

The wide-band semiconductors $AsCs_3Se_4$, Al_2HgSe_4, $C_2Te_2F_4$, $PdPbF_4$, $AlMoVO_7$ and Ag_6SiSO_8 have the total bandgap vary from 3.26 to 3.51 eV (see Table S1). Figure S5(a-f) shows the calculated band structure with IB of $AsCs_3Se_4$, Al_2HgSe_4, $C_2Te_2F_4$, $PdPbF_4$, $AlMoVO_7$ and Ag_6SiSO_8 respectively. The calculated values of E_{vi}, E_{ci}, ΔE_i and the total bandgaps are presented in . The bandgap types of over six compounds are the direct bandgap except for the indirect bandgap of $C_2Te_2F_4$ and $PdPbF_4$. From figure S5b, the calculated values for Al_2HgSe_4 are: total direct bandgap is 3.28 eV, whereas the bandgap E_{vi} is 1.41 eV. The transition between IB to CB is fast because the bandgap E_{ci} is 0.04 eV. However, the width of IB is 1.83 eV, ΔE_i in Al_2HgSe_4, which is much higher than E_{ci} and E_{vi}.

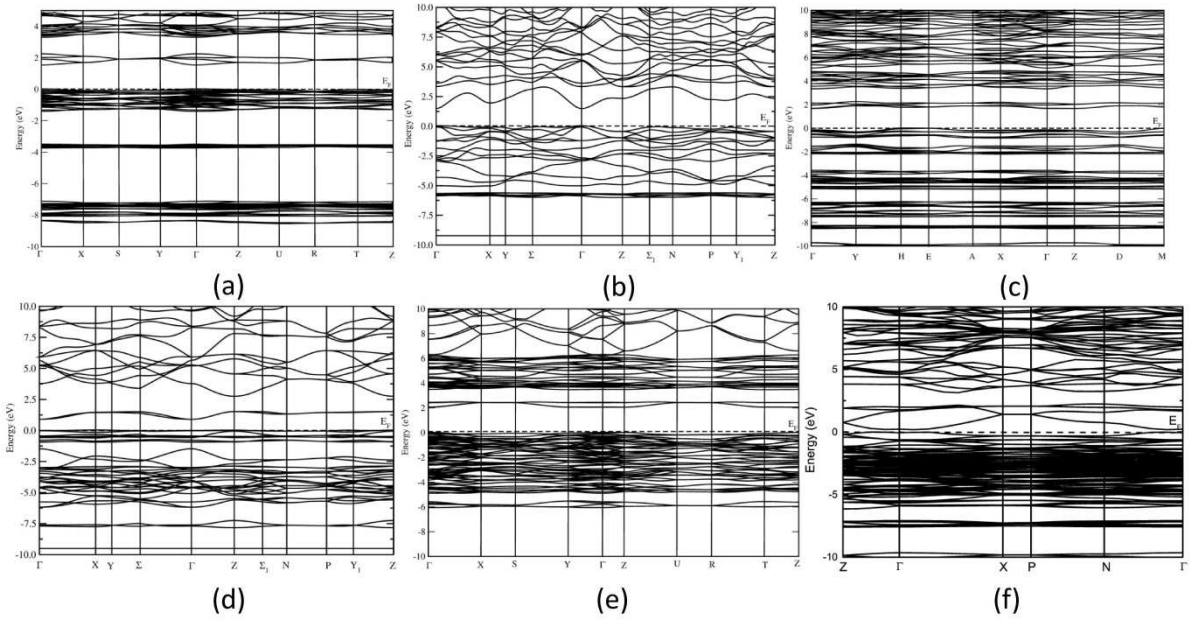

Figure S 1 Calculated electronic band structure of (a) $AsCs_3Se_4$, (b) Al_2HgSe_4, (c) $C_2Te_2F_4$ and (d) $PdPbF_4$. (e) $AlMoVO_7$ and (f) Ag_6SiSO_8. The fermi level is set to zero.

Table S1. Wide-band 2 semiconductors with intermediate band ranging from 3.15 eV to 3.51 eV

Serial no.	Chemical Formula	Pearson symbol	Space group number	Bandgap (E_{vi})	Bandgap (E_{ci})	Width of IB ΔE_i	Total Bandgap (Eg)	Bandgap type
1.	$AsCs_3Se_4$	oP32	62	1.49	1.04	0.73	3.26	DB
2.	Al_2HgSe_4	tI14	121	1.41	0.04	1.83	3.28	DB
3.	$C_2Te_2F_4$	mP32	4	1.67	1.08	0.58	3.33	ID
4.	$PdPbF_4$	tI24	140	1.92	0.8	0.61	3.33	ID
5.	$AlMoVO_7$	oP40	62	2.31	0.72	0.46	3.49	DB
6.	Ag_6SiSO_8	tI64	141	0.16	0.71	2.64	3.51	DB

Ground state structure of Ag_2ZnSnS_4:

In literature two types of tetragonal structures I-4 (kesterite-type; space group 82) and I-42m (stannite-type; space group 121) are described for Ag_2ZnSnS_4. Both of these two modifications are having similar atomic arrangement (see **Figure S 2**) and are highlighted by square box in **Figure S 2**. Our total energy calculation predicted that kesterite-type structure is energetically favourable for Ag_2ZnSnS_4 compound (see **Figure S 3**). This finding is consistence with the recent experimental findings by Gong *et al*. **[1]** The calculated structural parameters and atomic positions are well fitted with the experimental findings. The involved energy difference between the two structures is 0.14 eV/f.u.

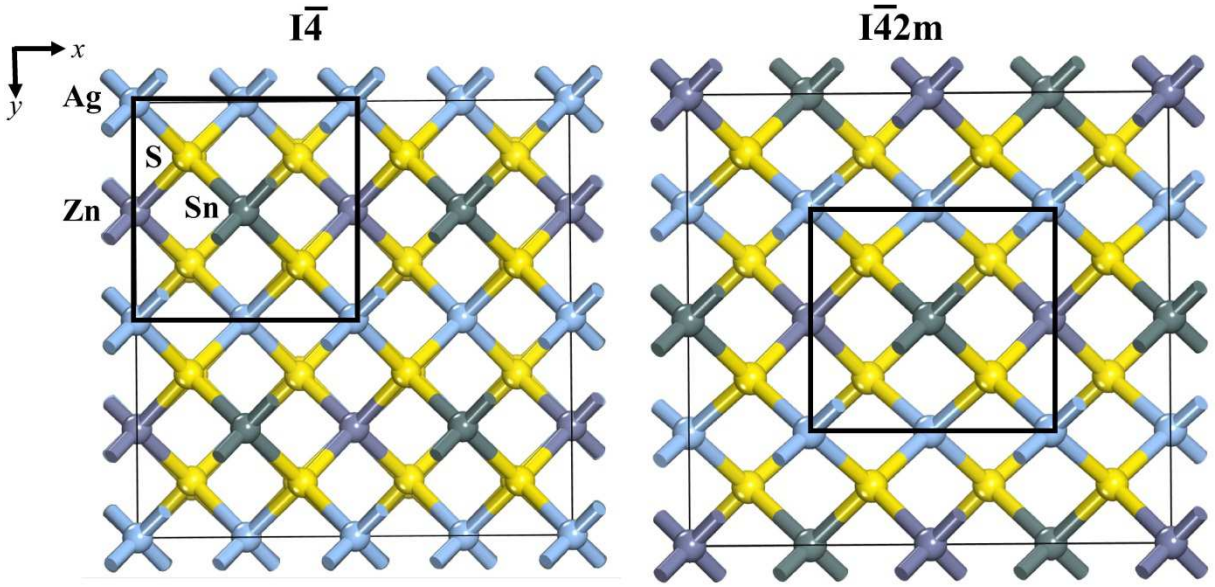

Figure S 2 *Crystal structures of tetragonal Ag_2ZnSnS_4 in I-4and I-42m structure viewed along [001]. Both of these two modifications are having similar atomic arrangement and are highlighted by square box. The atomic label for the different kinds of atoms is given in the illustration.*

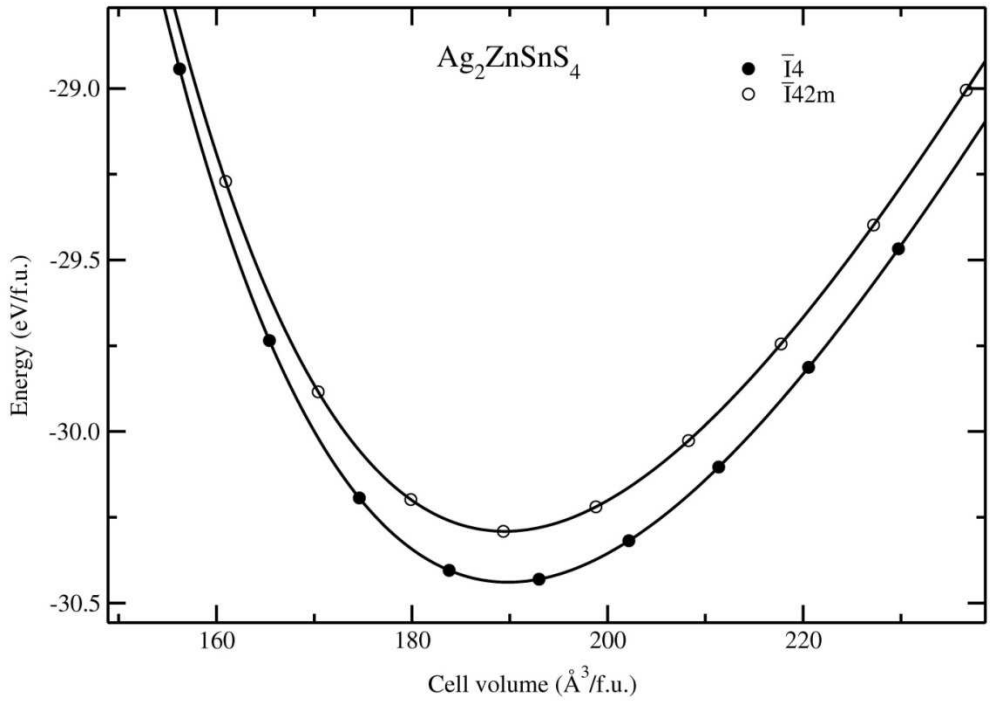

Figure S 3 *Calculated unit cell volume vs. total energy (per formula unit; f.u.) curves for Ag_2ZnSnS_4 in I-4and I-42m structure arrangements; structure types are labelled on the illustration.*

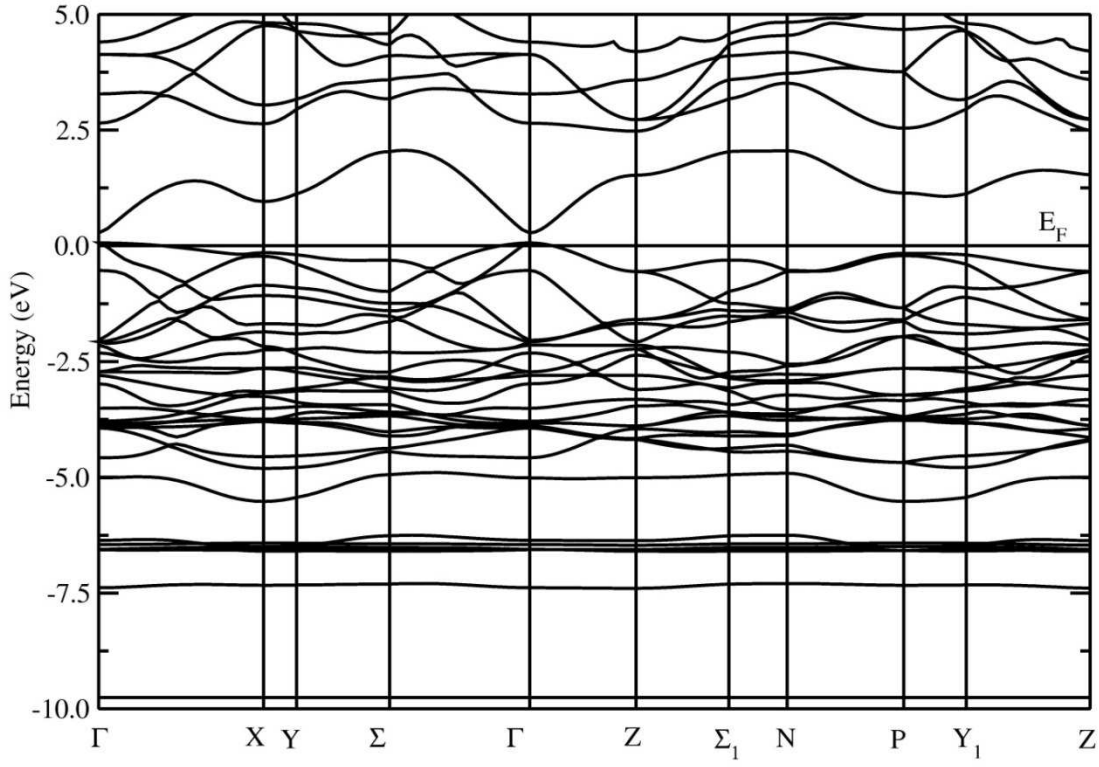

Figure S 4 *Band structure of tetragonal Ag_2ZnSnS_4 in I-4 space group. The Fermi level is set to zero.*

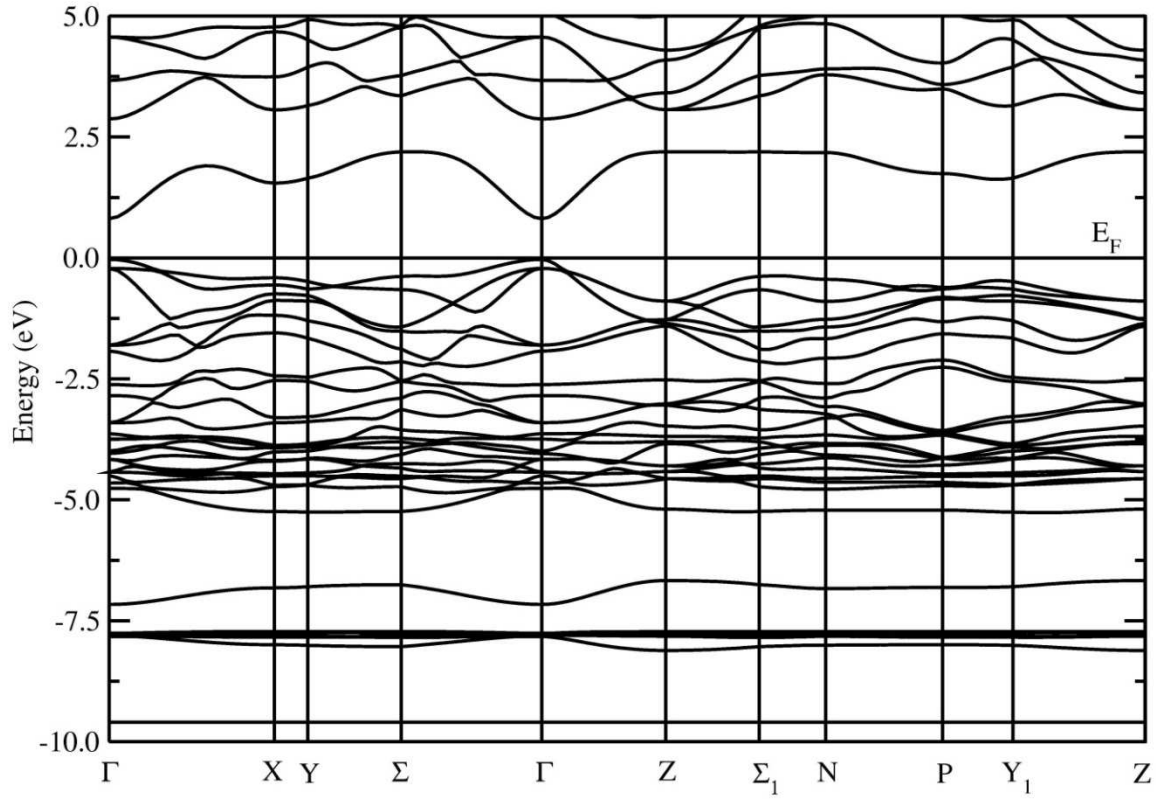

Figure S 5 *Band structure of tetragonal Ag_2ZnSnS_4 in I-42m space group. The Fermi level is set to zero.*

Table S2 List of Compounds with Intermediate band considered in this study are listed bellow. The chemical formula, pearson symbol, space group number, E_{vi}- Energy gap between top of the valence band to bottom of an intermediate band, E_{ci}- Energy gap between top of the intermediate band to bottom of the conduction band, Ei1-Ei2- gap between two IBs, ΔE_{i1} and ΔE_{i2}- bandwidth of the intermediate bands , Eg-total bandgap between top of the valence band and bottom of the conduction band, ID-indirect bandgap type, DB-direct bandgap type are listed

Serial no.	Chemical Formula	Pearson symbol	Space group number	Bandgap (E_{vi})	Bandgap (E_{ci})	Multibands gap (Ei1-Ei2)	Width of IBss ΔEi1, ΔEi2	Total Bandgap (Eg)	Band gap type
1.	$AgAsSe_2$	hR4	166	0.13	0.02	-	3.66	3.81	ID
2.	$AgClO_4$	tI12	121	3.60	0.57	0.13	2.59, 2.28	9.17	ID
3.	$AgPXe_2F_{10}$	tI56	140	2.48	0.72	2.39	0.99, 1.12	7.7	DB
4.	AgF_2	oP12	61	1.03	1.15	-	1.43	3.61	DB
5.	AgF_3	hP24	178	1.24	4.13	-	0.77	6.14	DB
6.	$AgKF_4$	tI24	140	2.13	4.12	-	0.19	6.44	DB
7.	$AgNaF_4$	tI24	140	1.78	4.01	-	0.36	6.15	DB
8.	$AgIO_4$	tI24	88	0.77	1.27	1.59	2.13, 3.26	9.02	ID
9.	$AgTcO_4$	tI24	88	2.34	0.35	0.8	0.98, 3.45	7.92	ID
10.	Ag_2GeBaS_4	tI16	121	0.90	0.35	-	1.16	2.41	ID
11.	Ag_2HgI_4	tI14	121	1.43	1.31	-	0.89	3.63	DB
12.	Ag_2KSbS_4	tI16	121	0.81	1.08	-	0.94	2.93	ID
13.	Ag_2ZnSnS_4	tI16	121	0.47	0.57	-	1.66	2.70	DB
14.	Ag_4TeSO_4	cP40	198	1.06	0.44	-	2.17	3.67	DB
15.	Ag_6SiSO_8	tI64	141	0.16	0.71	-	2.64	3.51	DB
16.	$AlAsO_4$	tI12	121	4.22	1.82	-	1.92	7.96	DB
17.	$AlH_{12}N_3O_{15}$	cI248	206	3.38	1.22	-	0.58	5.18	DB

18.	Al_2HgS_4	tI14	121	2.0	0.03	-	1.64	3.64	ID
Serial no.	Chemical Formula	Pearson symbol	Space group number	Bandgap (E_{vi})	Bandgap (E_{ci})	Multibands gap (Ei1-Ei2)	Width of IBs ΔEi1, ΔEi2	Total Bandgap (Eg)	Band gap type
19.	$AsBiO_4$	tI24	88	2.81	0.6	-	4.08	7.49	ID
20.	Al_2HgSe_4	tI14	121	1.41	0.04	-	1.83	3.28	DB
21.	$AsBO_4$	tI12	82	4.25	1.72	-	1.48	7.45	ID
22.	$AsCsF_4$	mP12	4	4.62	0.39	-	1.04	6.05	DB
23.	$AsCsF_6$	hR8	148	5.11	3.49	-	0.67	9.27	DB
24.	$AsCuF_7$	oI36	74	2.18	2.06	1.01	0.85, 1.17	7.27	DB
25.	$AsDyO_4$	tI24	141	3.61	0.65	-	2.04	6.30	DB
26.	AsF_3	oP16	33	5.15	0.28	-	2.79	8.22	ID
27.	AsF_5	hP12	194	4.55	3.82	-	0.88	9.25	DB
28.	AsF_6I_5	mS48	15	1.39	2.11	1.22	0.59, 0.27	5.58	DB
29.	$AsInF_6$	hR8	148	3.33	2.25	1.53	0.65, 1.26	9.02	ID
30.	$AsK1F_6$	hR8	166	4.76	3.63	-	0.90	9.29	DB
31.	$AsRbF_6$	hR8	166	4.94	3.60	-	0.75	9.29	DB
32.	$AsTlF_6$	hR8	148	4.56	1.55	-	0.64	6.75	ID
33.	$AsKrF_7$	mP36	14	2.44	3.79	2.32	0.17, 0.48	9.20	DB
34.	AsH_6NO_4	tI48	122	4.12	1.16	-	1.9	7.18	ID
35.	$AsHoO_4$	tI24	141	3.60	0.73	-	2.04	6.37	DB
36.	$AsLuO_4$	tI24	141	3.50	0.89	-	2.06	6.45	DB
37.	$AsTbO_4$	tI24	141	3.64	0.63	-	2.04	6.31	DB
38.	$AsYO_4$	Ti24	141	3.65	0.54	-	1.93	6.12	DB
39.	$As2Cl_4F_6$	tP24	85	2.84	2.34	2.35	0.22, 0.75	8.50	ID

Serial no.	Chemical Formula	Pearson symbol	Space group number	Bandgap (E_{vi})	Bandgap (E_{ci})	Multibands gap (Ei1-Ei2)	Width of IBs ΔEi1, ΔEi2	Total Bandgap (Eg)	Band gap type
40.	$As_4C_4F_{12}$	tP40	137	3.31	0.43	-	2.84	6.58	DB
41.	$As_3Mg_4NaO_{12}$	tI80	122	3.19	1.13	-	2.60	6.92	DB
42.	$As2KF_7$	mP40	14	4.78	0.28	-	2.92	7.98	DB
43.	$AuLiF_4$	mP24	15	2.59	0.41	2.41	0.37, 2.84	8.62	DB
44.	$AuLiF_4$	mS24	15	2.60	0.45	2.36	0.43, 2.9	8.74	ID
45.	$AuKF_6$	hR8	166	2.20	4.43	-	0.39	7.02	ID
46.	$AuTlF_6$	tP64	92	1.80	0.41	1.17	3.4, 1.94	8.72	ID
47.	Au_2BaO_4	tI28	88	1.69	0.11	-	1.77	3.57	ID
48.	$Au_2Cs_2Br_6$	tI20	139	0.67	1.23	-	0.81	2.71	DB
49.	Au_2CaF_{12}	tP15	99	1.72	4.31	-	0.84	6.87	DB
50.	Au_2CaO_4	tI28	88	1.81	0.18	-	1.65	3.64	ID
51.	Au_2CdF_{12}	mS60	12	2.0	2.72	-	0.36	5.08	DB
52.	Au_2CdF_8	tP22	127	2.33	1.2	-	0.72	4.25	DB
53.	$Au_2Cs_2Cl_6$	tI20	xx	0.93	1.72	-	0.73	3.38	DB
54.	Au_2CsF_7	mS40	15	2.29	2.07	0.38	0.21, 0.12	5.07	DB
55.	$Au_2Cs_2I_6$	tI20	139	0.64	1.01	-	0.7	2.35	ID
56.	Au_2HgF_8	tP22	127	2.1	0.21	1.21	2.88, 2.25	8.65	DB
57.	Au_2MgF_8	mP22	14	2.45	0.79	2.26	0.5, 2.94	8.94	DB
58.	Au_2NiF_8	mP22	14	2.24	0.41	1.58	0.63, 3.57	8.43	DB
59.	Au_2ZnF_8	mP22	14	2.24	0.02	1.85	0.65, 3.25	8.01	DB
60.	Au_3LaF_{12}	hR32	167	2.55	0.39	2.59	0.22, 1.95	7.70	ID
61.	$BClF_6$	mP32	14	3.32	4.37	-	0.65,	8.34	DB

Serial no.	Chemical Formula	Pearson symbol	Space group number	Bandgap (E_{vi})	Bandgap (E_{ci})	Multibands gap (Ei1-Ei2)	Width of IBs ΔEi1, ΔEi2	Total Bandgap (Eg)	Band gap type
62.	BSF_7	oP36	62	4.94	1.22	1.75	0.34, 0.43	8.68	DB
63.	$BN1F_8$	oP40	57	2.91	3.34	1.4	0.18, 0.16	7.99	DB
64.	B_2F_4	mP12	14	4.9	2.01	-	0.09	7.00	DB
65.	$Co_4B_6O_{13}$	cI46	217	3.72	0.89	-	2.25	6.86	ID
66.	$Zn_4B_6O_{13}$	cI46	217	4.04	1.97	-	1.12	7.13	ID
67.	BiF_5	tI12	87	1.98	3.73	-	1.38	7.09	ID
68.	BrF_3	oS16	36	2.17	3.08	0.8	0.49, 0.7	7.24	ID
69.	BrF_5	oS24	63	3.47	3.35	1.36	0.39, 0.49	9.06	ID
70.	$Ca_2U_6K_8O_{24}$	cI40	229	2.95	0.37	-	1.90	5.22	ID
71.	$Ca_3Te_2Zn_3O_{12}$	cI160	230	2.46	1.74	-	1.68	5.88	ID
72.	$CdPdF_6$	aP8	148	2.27	1.72	2.26	0.52, 1.91	8.69	ID
73.	$CdPtF_6$	hR8	148	2.74	0.95	0.68	0.66, 2.33	7.36	DB
74.	$CdSnF_6$	hR8	148	3.59	0.76	0.95	2.01, 1.93	9.24	ID
75.	$CdTiF_6$	hR8	148	4.92	0.98	0.79	0.24, 2.55	9.48	ID
76.	Cd_4OF_6	tP22	137	2.09	0.36	-	5.28	7.73	DB
77.	$Cd_4P_6N_{12}S$	cI46	217	3.08	0.42	-	0.87	4.37	ID
78.	$CeZrF_7$	mP18	4	4.24	1.05	-	0.28	5.57	ID
79.	SnClF	oP12	62	3.47	1.58	-	3.09	8.14	DB
80.	ClF	mP8	14	2.13	3.87	-	1.07	7.07	DB
81.	ClF_3	oP16	62	2.59	2.77	1.58	0.3, 0.73	7.97	ID
82.	$SbClF_8$	aP20	2	3.17	3.46	0.97	0.81, 0.72	9.13	ID
83.	$Hg_3 Se_2Cl_2$	cI28	199	1.75	0.65	-	1.92	4.32	ID

Serial no.	Chemical Formula	Pearson symbol	Space group number	Bandgap (E_{vi})	Bandgap (E_{ci})	Multibands gap (Ei1-Ei2)	Width of IBs ΔEi1, ΔEi2	Total Bandgap (Eg)	Band gap type
84.	$Hg_3Te_2Cl_2$	cI28	199	1.90	0.41	-	1.6	3.91	DB
85.	Li_2ZnCl_4	cF56	227	4.56	0.58	-	1.73	6.87	DB
86.	CoF_3	hR8	167	1.49	2.44	-	3.10	7.03	ID
87.	$CrNbF_6$	tI16	139	1.34	0.19	-	1.26	2.79	DB
88.	$CsCuF_4$	tI24	140	1.82	4.60	-	0.11	6.53	ID
89.	$CsHgF_3$	cP5	221	0.75	1.00	-	4.61	6.36	DB
90.	Cs_2HgF_4	tI14	139	2.05	0.88	-	2.56	5.49	ID
91.	$Cs2GeF_6$	cF36	225	6.01	1.64	-	1.08	8.73	DB
92.	$Cs_3Tl\ F_6$	tI20	139	3.34	1.78	-	0.78	5.90	ID
93.	CuF_2	mP6	14	1.75	0.98	-	1.38	4.11	DB
94.	HOF	oP12	19	3.23	2.91	-	0.66	6.80	ID
95.	PbIF	tP6	129	2.17	0.53	-	3.45	6.15	DB
96.	NOF	oP12	19	3.21	3.06	1.78	0.24, 0.64	8.93	ID
97.	TcO_3F	mP20	14	2.48	1.06	1.74	1.09, 1.55	7.92	ID
98.	HNF_2	oP16	29	4.41	0.88	-	1.62	6.91	DB
99.	PHF_2	oP16	19	3.83	0.36	0.73	2.43, 1.64	8.99	ID
100.	HgF_2	cF12	225	0.98	3.21	-	4.08	8.27	DB
101.	KrF_2	tP6	136	2.79	4.13	-	0.59	7.51	ID
102.	KrF_2	tI6	139	2.89	4.08	-	0.80	7.77	ID
103.	Pb_2OF_2	tP20	105	0.89	0.36	-	6.3	7.55	ID
104.	$SeOF_2$	oP16	29	4.15	0.88	0.99	1.63, 1.00	8.65	DB
Serial no.	Chemical Formula	Pearson symbol	Space group	Bandgap (E_{vi})	Bandgap	Multibands gap	Width of IBs	Total Bandgap	Band gap type

			number		(E_{ci})	(Ei1-Ei2)	ΔEi1, ΔEi2	(Eg)	
105.	XeF_2	tI6	139	2.74	3.60	-	0.88	7.22	ID
106.	FeF_3	cF64	227	2.80	1.34	-	2.26	6.40	ID
107.	FeF_3	hR8	167	2.71	1.14	-	2.44	6.29	DB
108.	FeF_3	hR32	167	2.77	1.19	-	2.40	6.36	DB
109.	IF_3	oP16	62	1.78	2.10	0.39	1.36, 1.58	7.21	ID
110.	NiF_3	hR8	167	1.24	2.54	2.84	0.62, 0.17	7.41	ID
111.	RhF_3	hP12	150	1.30	1.61	0.16	1.00, 1.56	5.63	ID
112.	$N_2H_8F_4$	hR14	166	5.27	1.27	-	0.53	7.07	ID
113.	HfF_4	mS60	15	5.39	0.31	-	1.50	7.20	ID
114.	K_2PdF_4	mS14	12	3.09	1.48	-	0.19	4.76	ID
115.	$NaSbF_4$	mP24	14	4.34	0.33	-	2.40	7.07	ID
116.	Na_2PdF_4	mP14	14	2.67	1.46	-	0.13	4.26	ID
117.	$TcOF_4$	hP36	176	1.97	1.49	1.35	0.59, 1.44	6.84	DB
118.	PdF_4	oF40	109	1.05	4.67	-	1.28	7.00	ID
119.	SnF_4	tI10	139	2.74	1.47	-	3.77	7.98	ID
120.	VF_4	mP10	14	1.92	1.74	-	3.61	7.27	DB
121.	XeF_4	mP10	14	2.81	4.10	0.04	0.57, 0.26	7.78	DB
122.	$KTeF_5$	oP28	57	5.24	1.14	-	1.20	7.58	DB
123.	$NaTeF_5$	oP28	62	5.25	1.21	-	1.36	7.82	ID
124.	Sn_2OF_5	mS32	12	1.56	1.10	0.25	1.51, 1.32	5.74	ID
125.	$PdRb_3F_5$	tP18	127	2.87	1.51	-	0.05	4.43	ID
126.	$SbSrF_5$	oP28	57	4.77	0.70	-	2.02	7.49	ID
Serial no.	Chemical Formula	Pearson symbol	Space group	Bandgap (E_{vi})	Bandgap	Multibands gap	Width of IBs	Total Bandgap	Band gap type

			number		(E_{ci})	(Ei1-Ei2)	ΔEi1, ΔEi2	(Eg)	
127.	Rb_2GeF_6	hP9	164	5.77	2.30	-	1.10	9.17	ID
128.	Rb_2GeF_6	cF36	225	5.94	1.96	-	1.22	9.12	DB
129.	$KNbF_6$	tP16	116	5.60	2.22	-	0.12	7.94	ID
130.	$LiNbF_6$	hR8	148	5.48	2.60	-	0.21	8.29	DB
131.	Li_2TiF_6	tP18	136	4.88	1.58	1.54	0.16, 0.31	8.47	DB
132.	MoF_6	oP28	62	4.06	1.06	3.84	0.11, 0.16	9.23	DB
133.	MoF_6	cI14	229	4.10	0.49	3.78	0.12, 0.38		ID
134.	$P_3N_3F_6$	oP48	62	5.69	0.24	-	1.51	7.44	DB
135.	$NiSrF_6$	hR8	166	1.65	5.88	-	0.44	7.97	DB
136.	Sn_2F_6	cF32	221	2.26	0.54	1.01	2.06, 1.20	7.07	ID
137.	TeF_6	oP28	62	4.37	4.58	-	0.54	9.49	DB
138.	WF_6	oP28	62	5.04	3.79	-	0.14	8.97	DB
139.	Xe_2F_6	mP16	14	2.56	3.97	0.51	0.22, 0.29	7.55	ID
140.	K_2NbF_7	mP40	62	4.93	0.68	1.48	0.10, 0.13	7.32	DB
141.	K_2PaF_7	mS40	15	3.99	2.84	-	0.64	7.47	ID
142.	K_2TaF_7	oP40	62	5.68	1.05	-	0.17	6.90	DB
143.	$NiRb_3F_7$	tP22	127	0.78	4.91	-	0.15	5.84	ID
144.	Pb_2RhF_7	mP40	14	2.85	1.06	1.27	0.38, 3.01	8.57	DB
145.	$TiRb_3F_7$	tP22	127	3.52	1.80	-	0.04	5.36	DB
146.	$SbXeF_7$	mP36	14	2.79	3.44	1.69	0.27, 0.56	8.75	DB
147.	$SnTlF_7$	mP36	14	1.63	1.93	-	3.69	7.25	DB
148.	$SrTaF_7$	mP18	11	5.66	0.21	1.46	0.19, 0.25	7.77	ID
Serial no.	Chemical Formula	Pearson symbol	Space group	Bandgap (E_{vi})	Bandgap	Multibands gap	Width of IBs	Total Bandgap	Band gap type

			number		(E_{ci})	(Ei1-Ei2)	ΔEi1, ΔEi2	(Eg)	
149.	$Pb_5I_2F_8$	hR15	160	2.90	0.87	-	3.53	7.30	ID
150.	K_3TaF_8	hP24	186	3.98	0.09	1.48	0.06, 0.30	5.91	DB
151.	Sn_3F_8	mP22	14	2.70	0.83	0.85	0.95, 3.06	8.39	DB
152.	$NbSeF_9$	hR44	146	5.53	1.99	0.68	0.62, 0.09	8.91	DB
153.	$Na_3Ga_3Te_2O_{12}$	cI160	230	1.91	0.97	-	2.00	4.88	DB
154.	Hg_3TeO_6	CI160	230	0.59	0.39	-	3.90	4.88	DB
155.	LiO_3I	tP40	86	3.59	0.68	-	3.11	7.38	DB
156.	LiO_3I	hP10	173	3.65	2.04	-	2.53	8.22	ID
157.	K_3SbS_4	cI16	217	2.14	1.58	-	0.39	4.11	ID
158.	Li_2WO_4	tI12	141	4.12	1.43	-	0.97	6.52	DB
159.	Li_3NbO_4	cI64	197	4.03	1.65	-	1.17	6.85	DB
160.	$Li_3Nd_3W_2O_{12}$	cI160	230	3.28	0.22	-	0.96	4.46	DB
161.	Li_3TaO_4	mS64	15	4.66	0.69	-	1.18	6.53	ID
162.	Li_3VO_4	oP16	31	4.02	0.59	0.49	0.20, 0.80	6.10	ID
163.	$Li_6Zr_2O_7$	mS60	15	3.92	0.50	-	2.40	6.82	DB
164.	Li_7TaO_6	aP14	146	4.56	0.25	-	0.64	5.45	ID
165.	$Zn_8P_{12}N_{24}O_2$	cI46	217	3.44	0.57	-	0.25	4.26	ID
166.	Na_3SbS_4	cI16	217	1.92	1.27	-	0.42	3.61	ID
167.	Na_3SbSe_4	cI16	217	1.02	1.24	-	0.71	2.97	DB
168.	$ZnSr_2WO_6$	cF40	225	3.05	1.31	-	1.01	5.37	ID
169.	$AgBiSe_2$	hR4	166	0.44	0.08	-	3.36	3.88	ID
170.	$AgBiTe_2$	hR4	166	0.17	0.09	-	3.27	3.53	ID
Serial no.	Chemical Formula	Pearson symbol	Space group	Bandgap (E_{vi})	Bandgap	Multibands gap	Width of IBs	Total Bandgap	Band gap type

			number		(E_{ci})	(Ei1-Ei2)	ΔEi1, ΔEi2	(Eg)	
171.	$AgCN_3O_2$	oP28	57	3.18	0.61	-	0.46	4.25	DB
172.	$AgCuPO_4$	oP56	61	1.27	0.61	-	0.74	2.62	DB
173.	AgK_2SbS_4	oP32	118	1.52	1.03	-	0.47	2.97	DB
174.	AgN_3O_4	oP64	61	2.67	1.19	1.04	0.28, 2.18	7.36	DB
175.	AgP_4TaO_{13}	oP76	19	3.41	0.70	-	0.49	4.60	DB
176.	Ag_3AsS_4	oP16	31	0.73	1.04	-	1.00	2.77	DB
177.	$AlAsH_4O_6$	oP96	61	3.66	1.2	-	2.19	7.05	DB
178.	$AlCl_4NS_2$	oP32	62	2.14	0.13	2.88	0.10, 0.4	5.65	DB
179.	$AlCsSiO_4$	oP28	36	1.21	2.07	-	1.39	4.54	DB
180.	$AlMoVO_7$	oP40	62	2.31	0.72	-	0.46	3.49	DB
181.	$Al_2Ca_2Sn_2O_9$	oP60	60	2.45	0.78	-	2.91	6.14	DB
182.	$Al_5NaTi_2O_{12}$	oP40	55	3.13	0.54	-	1.27	4.94	DB
183.	$AsCl_3$	oP16	19	4.04	1.97	-	0.84	6.85	ID
184.	AsCoSe	oP24	61	0.46	0.30	-	4.43	5.19	ID
185.	$AsCs_3Se_4$	oP32	62	1.49	1.04	-	0.73	3.26	DB
186.	$AsZn_2HO_5$	oP36	58	2.65	1.01	-	2.71	6.37	ID
187.	$AsLiZnH_2O_5$	oP40	33	3.41	0.83	-	2.22	6.46	DB
188.	$AsNaH_4O_5$	oP44	19	3.87	1.33	-	1.92	7.12	ID
189.	$AsNH_6O_4$	oP48	19	3.41	1.00	-	1.71	6.12	DB
190.	$AsLiMgO_4$	oP28	62	3.46	1.28	-	2.00	6.74	DB
191.	$AsLiNiO_4$	oP28	62	2.79	1.03	-	2.35	6.17	DB
192.	$AsLi_2NaO_4$	oP16	31	3.92	1.51	-	1.82	7.25	ID
Serial no.	Chemical Formula	Pearson symbol	Space group	Bandgap (E_{vi})	Bandgap	Multibands gap	Width of IBs	Total Bandgap	Band gap type

			number		(E_{ci})	(Ei1-Ei2)	ΔEi1, ΔEi2	(Eg)	
193.	$AsRbSnO_5$	oP64	33	1.83	0.72	-	3.94	6.49	DB
194.	$AsSbO_5$	oP28	19	1.77	1.00	-	4.22	6.99	DB
195.	$AsRb_3Se_4$	oP32	62	1.32	0.98	-	0.97	3.15	DB
196.	$As_2MgXe_2F_{16}$	oP42	55	2.98	3.27	0.93	0.44, 0.6	8.22	DB
197.	As_2O_5	oP28	92	1.46	1.17	-	6.65	9.28	DB
198.	Au $K1C_4$ N_4H_2O	oP52	19	4.29	1.17	0.3	0.05, 0.36	5.87	DB
199.	$BaTe_2F_{10}$	mS52	15	4.90	1.93		1.15	7.98	ID
200.	$BaZr_2F_{10}$	mS52	15	5.75	0.37		1.47	7.59	ID
201.	$BaSb_2F_{12}$	aP15	1	4.07	2.65	1.06	0	7.78	DB
202.	$BaSbF_5$	oP28	57	4.73	0.22		1.84	6.79	ID
203.	$BaGeF_6$	hR8	166	5.55	3.11		0	8.66	DB
204.	$BaNiF_6$	hR8	166	1.72	6.01		0.37	8.09	DB
205.	$BaPbF_6$	hR8	166	2.86	5.02		0	7.88	DB
206.	$BaSnF_6$	hR8	148	4.98	3.52		0	8.50	DB
207.	$BaTeF_6$	oF128	43	4.79	1.67		1.26	7.72	ID
208.	$BaTiF_6$	hR8	166	4.80	0.94	1.6	0.14, 0.33	7.81	ID
209.	$BaZrF_6$	mP32	14	6.32	0.41	0.274	0.53, 0.146	7.68	DB
210.	$BaZrF_6$	oS32	67	6.26	0.35	-	0.64	7.25	ID
211.	$BaTm_2F_8$	mS22	12	1.98	5.36		0	7.34	ID
212.	Ba_2PdF_6	oS36	64	2.84	2.04	-	4.88	9.76	ID
213.	Ba_2ZrF_8	oP44	62	5.95	1.1	-	0	7.05	DB
214.	Ba_2SrTeO_6	hR10	225	3.16	1.96	-	5.12	10.24	ID
Serial no.	Chemical Formula	Pearson symbol	Space group	Bandgap (E_{vi})	Bandgap	Multibands gap	Width of IBs	Total Bandgap	Band gap type

			number		(E_{ci})	(Ei1-Ei2)	ΔEi1, ΔEi2	(Eg)	
215.	$Ba_3In_2F_{12}$	tP34	127	4.70	0.9	0.52	1.1, 0.28	7.50	DB
216.	$BiClF_8$	aP20	2	2.22	4.12	0.82	0.36, 0.83	8.35	DB
217.	$BiCsF_6$	hR8	148	2.92	5.5	-	0	5.5	DB
218.	$BiKF_6$	tP16	116	2.90	5.2	-	0.35	8.45	DB
219.	$BiLiF_6$	hR8	148	2.75	6.14	-	0	8.89	DB
220.	$BiNaF_6$	hR8	148	2.89	5.74	-	0	8.63	ID
221.	$BiRbF_6$	hR8	148	2.79	5.61	-	0	8.40	DB
222.	$BiKrF_7$	mP36	14	2.438	5.11	0.38	0.212, 0.41	8.55	DB
223.	$BiNa_3O_3$	cI56	217	2.89	0.37	0.65	1.3, 1.58	6.79	DB
224.	$Bi_{24}Pb_2O_{40}$	cI66	197	1.52	1.4	0.73	5.63	9.28	ID
225.	$Bi_4Si_3O_{12}$	cI76	220	3.93	1.59	-	2.1	7.62	DB
226.	$CsBrF_6$	hR8	148	4.03	3.34	-	0.31	7.68	DB
227.	PbBrF	tP6	129	2.72	0.33		3.82	6.75	DB
228.	Sn_3BrF_5	mP36	14	3.21	0.3	-	3.96	7.47	DB
229.	$CsBr_2F$	tP4	123	1.77	1.34	-	1.41	4.52	DB
230.	$GeBr_2F_{10}$	mP26	14	2.85	2.73	1.85	0.8,0.19	8.42	ID
231.	Hg_3Te2Br_2	cI28	199	1.73	0.47	-	1.48	3.68	DB
232.	CBr_3F	oP20	62	3.27	0.23	1.13	0.37, 0.92	5.92	DB
233.	$C_{12}SeF_{10}$	mP46	4	2.78	0.54	-	1.74	5.06	DB
234.	$C_{12}Ru_4Se_4O_{12}$	cI64	217	2.19	1.32	0.93	0, 1.33	5.77	ID
235.	$CClF_3$	oS20	36	6.55	0.7	-	0.47	7.72	ID
236.	CCl_2F_2	oF40	43	4.73	0.57	-	0.66	5.96	DB
Serial no.	Chemical Formula	Pearson symbol	Space group	Bandgap (E_{vi})	Bandgap	Multibands gap	Width of IBs	Total Bandgap	Band gap type

			number		(E_{ci})	(Ei1-Ei2)	ΔEi1, ΔEi2	(Eg)	
237.	CCl_3F	oP40	61	4.91	0.26	0.76	0.33, 0.62	6.88	DB
238.	CF_3I	oS40	64	3.71	1.78	-	0.37	5.86	ID
239.	ClF_7	mP36	14	4.65	2.41	-	1.22	8.28	DB
240.	$C_2O_3F_2$	oP56	19	5.27	0.68	-	0.47	6.42	DB
241.	$C_2Te_2F_4$	mP32	4	1.67	1.08	-	0.58	3.33	ID
242.	$C_2Te_2F_6$	mP40	14	2.41	1.01	0.22	0.35, 0.83	4.82	DB
243.	K_6C_{60}	cI132		0.61	0.28	-	0.39	1.28	ID
244.	$CaPdF_6$	hR8	148	2.62	4.51	-	0.24	7.37	ID
245.	$CaPtF_6$	hR8	148	3.17	2.77	-	0.25	6.19	ID
246.	$CaSnF_6$	hR8	148	4.85	4.07	-	0	8.92	DB
247.	$AgAsF_7$	P36	62	1.46	1.35	1.83	0.92,1.27	6.83	DB
248.	$AgSbF_6$	cI64	206	3.37	1.29	0.94	1.92, 1.45	8.97	DB
249.	$AgTiF_6$	aP8	2	1.46	0.89	2.64	0.52, 0.20	5.73	DB
250.	$AsNaF_6$	cF32	225	4.93	3.42	-	0.87	9.22	DB
251.	As_2MnF_{12}	tI60	141	4.01	1.4974	-	1.2119	6.7258	DB
252.	$AuTh_2F_{11}$	tI56	139	2.59	0.24	3.00	0, 1.67	7.51	DB
253.	PbF_4	tI10	139	1.86	3.31	-	3.15	8.32	ID
254.	$AuKF_4$	tI24	140	2.88	2.24	-	0.2614	5.39	DB
255.	$AuNaF_4$	tI24	140	2.61	2.03	-	0.401	5.05	DB
256.	$AuRbF_4$	tI24	140	2.96	2.227	-	0.23	5.42	DB
257.	Au_2BaF_{12}	cP60	224	1.79	1.03	3.12	0.7, 0.5	7.14	DB
Serial no.	Chemical Formula	Pearson symbol	Space group number	Bandgap (E_{vi})	Bandgap (E_{ci})	Multibands gap (Ei1-Ei2)	Width of IBs ΔEi1, ΔEi2	Total Bandgap (Eg)	Band gap type

258.	Au_2BaF_8	tI44	82	2.96	0.41	2.29	0.25, 2.38	8.29	ID
259.	$BaPdF_4$	tI24	140	2.56	1.74	-	0.39	4.69	ID
260.	$BaTaF_7$	cP72	205	5.79	1.49	-	0.21	7.49	DB
261.	$BiKF_4$	cF96	225	3.25	0.45	-	3.30	6.55	DB
262.	$BiKF_6$	cI64	206	2.90	5.07	-	0.58	8.55	ID
263.	$BrKF_4$	tI24	140	3.12	2.52	-	0.85	6.49	ID
264.	$BrRbF_4$	tI24	140	3.31	1.92	-	0.85	6.08	DB
265.	$Cs_2Br_2F_2$	tI12	139	2.52	2.05	-	0.26	4.83	ID
266.	$CaPdF_4$	tI24	140	2.22	1.89	-	0.49	4.60	DB
267.	$CaPbF_6$	cF32	225	3.41	4.63	-	0.64	8.68	DB
268.	$CaSnF_6$	cF32	225	4.82	3.28	-	0.8	8.9	DB
269.	$TaCl_4F$	tI48	82	3.21	0.49	1.72	0.58, 0.54	6.54	ID
270.	Cs_3TlF_6	tI20	139	3.32	1.73	-	0.8	5.85	ID
271.	KYb_3F_{10}	cF112	225	0.96	0.39	6.27	0.07, 0.81	8.5	DB
272.	KSb_4F_{13}	tI36	82	4.66	0.9	-	2.91	8.47	ID
273.	Rb_2HgF_4	tI14	139	1.96	0.37	-	2.81	5.14	DB
274.	$PbPdF_4$	tI24	140	1.92	0.8	-	0.61	3.33	ID
275.	$PdSrF_4$	tI24	140	2.37	1.8	-	0.43	4.60	DB
276.	Rb_2GeF_6	cF36	225	5.92	1.96	-	1.20	9.08	DB
277.	K_2NiF_6	cF36	225	2.22	5.2	-	0.33	7.75	ID
278.	$NaSbF_6$	cP32	225	4.86	3.38	-	0.9	9.14	DB
279.	$NiRb_2F_6$	cF36	225	2.29	4.90	-	0.24	7.43	ID
Serial no.	Chemical Formula	Pearson symbol	Space group number	Bandgap (E_{vi})	Bandgap (E_{ci})	Multibands gap (Ei1-Ei2)	Width of IBs ΔEi1, ΔEi2	Total Bandgap (Eg)	Band gap type

280.	$PdRb_2F_6$	cF36	225	2.84	3.69	-	0.29	6.82	DB
281.	Rb_3TlF_6	tI20	139	3.16	1.63	-	0.97	5.76	ID
282.	Pb_2F_6	tP16	116	1.96	1.10	2.40	1.23, 1.89	8.58	DB

List S1. List of computed compounds (in total 2100) considered in this study with their ICSD number:

$Ag_5Cl_3P_4S_6$-416586; Ag_6Ca_6N-78395; $AgAlO_2$-160643; $AgAlO_2$-99688; $AgAlS_2$-28744; $AgAlS_2$-604692; $AgAlS_2$-604694; $AgAlS_2$-604698; $AgAlSe_2$-28745; $AgAlSe_2$-604704; $AgAlSe_2$-604706; $AgAlTe_2$-28746; $AgAl_2Pr$-604688; $AgAsF_7$-62510; $AgAsHg_2O_4$-413087; $AgAsS_2$-18101; $AgAsSe_2$-20087; $AgAs_2Nd$-174360; $AgAs_2Pr$-98736; $AgAs_2Sm$-174361; $AgAuCl_6Cs_2$-26162; $AgAuF_4$-90071; $AgAuTe_2$-55250; $AgBF_4$-415320; $AgBF_5$-80645; $AgBF_5$-80646; AgBa-57342; $AgBaO_9P_3$-50672; $AgBe_2$-109313; $AgBiCr_2O_8$-8224; $AgBiCr_4O_4$-14233; $AgBiCr_4O_4$-14234; $AgBiO_3$-89432; $AgBiSe_2$-26518; $AgBiTe_2$-43266; AgBrHgS-411773; $AgBr_3Cs_2$-150288; $AgBr_3Rb_2$-150287; AgCN-85783; AgCNO-23833; AgCNO-260378; $AgCN_3O_2$-408288; $AgC_2F_6H_2N_2Sb$-63287; $AgC_2H_2N_3O$-63100; $AgC_2KN_2S_2$-280587; AgC_2N_3-68453; AgCaGe-421236; AgCaSb-56982; $AgCdO_4V$-401350; $AgCd_2GaS_4$-90459; $AgClO_2$-15407; $AgClO_3$-30227; $AgClO_4$-100280; $AgClO_4$-185363; $AgCl_3Cs_2$-150286; $AgCl_3Rb_2$-280031; $AgCrO_2$-4149; $AgCrS_2$-24797; $AgCrSe_2$-24799; $AgCrSe_2$-42397; $AgCrTe_2$-605002; $AgCsF_3$-23154; AgCsO-25745; AgCsO-49754; $AgCsSe_4$-87464; $AgCs_2F_4$-16254; $AgCs_2I_3$-150291; $AgCuO_4P$-35590; $AgCuO_4V$-419202; AgCuS-66581; $AgCuTe_2$-42482; $AgDySe_2$-605083; $AgErS_2$-423921; $AgErSe_2$-951; AgEu-58257; $AgEuO_4Ti$-78720; AgF_0PXe_2-412662; AgF_2Sb_2-65186; AgF_2Ta_2-62543; AgF_2-20453; AgF_2-6277; AgF_2-66014; AgF_3-80477; AgF_3Rb-23153; AgF_3Zn-28950; AgF_4K-72715; AgF_4K-9904; AgF_4Na-9903; AgF_6Pd-51507; AgF_6Sb-28676; AgF_6Sb-411795; AgF_6Ti-51506; AgF_7Ir-79880; $AgFeO_2$-31919; $AgFeO_6Se_2$-90414; $AgFeS_2$-156643; $AgFeS_2$-56263; $AgFeS_2$-605138; $AgGaSe_2$-28748; $AgGaTe_2$-605230; $AgGdSe_2$-602138; AgH_2O_4V-75941; AgH_4NS_4W-84370; $AgHf_2$-163152; AgHgIS-54796; $AgHg_2NO_5$-89685; $AgHg_2O_4P$-2208; $AgHg_3O_6Sb$-170764; $AgHoSe_2$-156419; $AgHoSe_2$-605365; $AgIO_4$-52380; $AgISe_3$-414116; $AgITe_3$-414117; AgI_2Tl-26318; AgI_3K_2-1969; AgI_3Rb_2-150290; AgI_3Tl_2-78929; $AgInO_2$-202429; $AgInS_2$-28750; $AgInS_2$-32655; $AgInS_2$-51618; $AgInSe_2$-28751; $AgInSe_2$-604401; $AgInTe_2$-28752; $AgIn_2$-58282; AgKO-188532; AgK_2S_4Sb-82144; AgLi-247145; $AgMnO_4V$-246202; $AgMo_6S_8$-600661; $AgMo_6Se_8$-600325; $AgNO_3$-1685; $AgNO_3$-374; AgN_3-183201; AgN_3O_4-419628; AgNaO-40153; $AgNbO_3$-55643; $AgNiO_2$-73974; $AgNiSe_2$-605616; $AgNiTe_2$-605619; AgO-202055; AgO_3P_4Ta-86892; AgORb-188533; AgORb-40155; AgORb-49753; AgO_2Rh-261561; AgO_2Sc-422442; AgO_2Yb-163472; AgO_3Sb-245292; AgO_3Ta-40830; AgO_4Re-280086; AgO_4Tc-281321; AgO_5SeV-417773; $AgPS_4Zn$-48197; $AgRbSe_4$-87463; AgS_2Yb-27090; AgS_2Yb-27091; $AgSbTe_2$-170663; AgSbYb-83983; $AgSc_6Te_2$-

94859; AgSeTl-100710; $AgSe_2Tb$-605827; AgSr-58358; AgTeTl-23367; $AgTe_2Y_6$-160181; $AgTe_3$-37186; $AgTh_2$-58367; AgYb-58377; $AgZr_2$-58391; $Ag_2Al_7Ca_3$-104173; Ag_2AsKO_4-409793; Ag_2BaGeS_4-10040; Ag_2BaGe_2-25318; Ag_2BaSn_2-25332; Ag_2BaTe_2-246048; Ag_2Ba_3-108847; Ag_2BiO_3-410665; Ag_2BrNO_3-1311; Ag_2CaGe_2-25316; Ag_2CdGeS_4-152753; Ag_2CeSi_2-106693; Ag_2CeSi_2-52551; Ag_2ClNO_3-8013; $Ag_2Cl_6Cs_2$-66067; Ag_2Cl_6Re-156662; Ag_2Cl_6Re-249357; Ag_2CrO_4-16298; $Ag_2Cu_2O_3$-51502; Ag_2Dy-57380; Ag_2Er-58252; Ag_2EuSi_2-106697; Ag_2FeS_4Sn-42534; Ag_2Gd-104473; Ag_2GdSi_2-52574; Ag_2GeO_3-167332; Ag_2Ge_2Nd-154451; Ag_2Ge_2Pr-154449; Ag_2Ge_2Sr-25317; $Ag_2H_3IO_6$-155415; $Ag_2H_4O_2S_3$-408949; Ag_2HgI_4-6069; Ag_2HgSe_4Sn-95094; Ag_2Ho-58278; Ag_2INO_3-8075; $Ag_2I_6O_8Ti$-420852; Ag_2KPS_4-420033; Ag_2KS_4Sb-82143; Ag_2LaSi_2-52587; $Ag_2La_2O_0Ti_3$-74194; Ag_2Lu-605531; Ag_2MnO_4-35762; Ag_2Nb_4O-180731; Ag_2NdSi_2-106695; Ag_2NiO_2-160574; $Ag_2O_0UW_2$-98550; Ag_2OTa_4-180734; Ag_2O_3Si-36589; $Ag_2P_2STi_2$-84606; Ag_2PrSi_2-106694; Ag_2S_4SnZn-605734; Ag_2Sc-605791; Ag_2Se-15213; Ag_2Si_2Sm-106696; Ag_2Si_2Sr-25330; Ag_2Si_2Tb-98339; Ag_2Si_2Yb-52607; Ag_2Sn_2Sr-414; Ag_2Sr_3-58360; Ag_2Tb-58365; Ag_2Tm-58373; Ag_2Y-605957; Ag_2Yb-605966; Ag_2Zr-605995; Ag_3AsS_3-27841; Ag_3AsS_3-38388; Ag_3AsS_4-86227; Ag_3AsSe_3-2426; Ag_3AsSe_3-82636; $Ag_3As_2K_3$-32016; Ag_3AuSe_2-15734; Ag_3AuTe_2-15733; Ag_3BO_3-26521; Ag_3Ca_5-57355; $Ag_3CeK_2Te_4$-86678; Ag_3CuS_2-163982; $Ag_3Ge_3P_6Sn_2$-52575; Ag_3NO_3Se-33581; Ag_3O_4V-417470; Ag_3PS_4-416585; Ag_3PSe_4-97760; $Ag_3P_6Si_3Sn_2$-52595; Ag_3S_2Tl-75976; Ag_3S_3Sb-64986; Ag_3Sb-52600; Ag_3Sn-2721; Ag_3Yb_5-58382; Ag_4EuSb_2-424312; $Ag_4I_2O_4Se$-418902; Ag_4Lu-58321; $Ag_4Mn_3O_8$-414178; $Ag_4N_2O_2S$-23111; Ag_4O_4STe-421880; $Ag_4P_2Se_6$-1727; Ag_4Sb_2Sr-424311; Ag_4Sc-58349; Ag_5Cd_8-604897; Ag_5IO_6-415893; Ag_5O_4Si-165377; Ag_5S_4Sb-36347; Ag_5Zn_8-58389; Ag_6BaO_4-9288; $Ag_6CeN_9O_{27}$-59256; Ag_6CrO_8Si-420804; $Ag_6Ge_0P_2$-70055; Ag_6O_4Sr-10359; Ag_6O_8SSi-6225; Ag_8Ca_3-107145; Ag_8GeS_6-100079; $Ag_8O_4S_2Si$-2330; Ag_8S_6Si-1054; Ag_8S_6Ti-95648; Ag_8Se_6Sn-95093; Al_0Ba_7-420092; $Al_2Ca_8O_{24}S_2$-67589; $Al_2Ca_8O_{24}Te_2$-86156; $Al_2Cd_8O_{24}S_2$-78368; $Al_2Cd_8O_{24}Te_2$-86155; Al_2Mg_7-163478; Al_2Mn-608472; Al_2Mo-608577; $Al_2O_{24}S_2Sr_8$-67590; $Al_2O_{24}Sr_8Te_2$-82609; Al_2Re-109107; Al_2Tc-58178; Al_2W-58207; $Al_4Ca_2O_{32}$-164634; Al_4Mg_3-150647; $Al_4O_{25}Sr_4$-88527; $Al_7Pd_8Si_4$-52650; $AlAsH_4O_6$-170740; $AlAsO_4$-24512; $AlAs_3Ca_3$-32727; AlAuCa-370015; AlAuYb-370027; $AlAu_2$-57496; $AlAu_2$-606020; $AlBMgO_4$-34349; $AlBO_3$-30538; $AlBO_4Pb$-98572; AlB_4Cr_3-20082; AlB_4Lu-41405; AlB_4Yb-181368; AlB_6Yb_2-41404; $AlBaF_5$-37033; $AlBaLaO_4$-62490; $AlBa_3F_9$-72718; $AlBa_3HO_4$-280520; $AlBeNa_3O_8Si_2$-4334; $AlBr_4Cs$-83435; AlCOSc-419683; $AlCaF_4Mg_3Na_3$-168054; $AlCaHO_5Si$-12127; $AlCaH_5$-156314; AlCaPd-370036; $AlCa_2ClF_2H_8O_2S_2$-80437; $AlCa_2F_7$-100308; $AlCa_3Sb_3$-36363; $AlCdF_6Na$-80559; $AlCeH_6$-247039; $AlCeO_3$-150277; $AlCeO_3$-245264; $AlCeO_3$-245267; $AlCePd_2$-604242; AlCePt-104635; AlCeRh-160052; AlCeRu-160051; $AlCl_3H_2O_6$-22071; $AlCl_4Cs$-8118; $AlCl_4Cu$-165607; $AlCl_4In$-170790; $AlCl_4NS_2$-27210; $AlCl_4Na$-2307; $AlCl_4Tl$-419828; $AlCr_2$-57651; $AlCsCuF_6$-240292; $AlCsO_4Si$-160822; $AlCs_2F_6Na$-41801; $AlCuF_6K$-59003; $AlCuO_2$-25593; $AlCuS_2$-28733; $AlCuSe_2$-28734; $AlCuTe_2$-28735; $AlCu_3$-151216; AlDy-57734; AlEu-107525; $AlFO_4Sr_3$-50736; AlF_3-130021; AlF_3-202681; AlF_3-29131; AlF_3-30274; AlF_3-38305; AlF_3-68826; AlF_3-72174; AlF_3-79816; $AlF_3K_2O_4S$-161272; AlF_4K-166825; AlF_4K-77913; AlF_4Rb-54122; AlF_4Tl-202455; $AlF_5H_0N_2O$-201652; $AlF_6H_2N_3$-96591; AlF_6K_3-262078; AlF_6Li_3-34672; AlF_6Na_3-74211; AlF_6PdRb-78749; $AlFeO_3$-203203; $AlGdO_3$-59848; AlGeLa-105149; $AlGeLi_3O_5$-72098; $AlGeO_5Y$-32744; AlGePr-90160; $AlGe_3Tb_2$-152747; $AlGe_3Y_2$-78969;

$AlH_2N_3O_5$-96765; $AlHO_2$-16768; AlH_2LiO_5Si-161494; AlH_4K-99082; AlH_4K-99083; AlH_4Na-8022; AlH_4Th_2-43313; AlH_5Mg-165987; AlH_5Sr-156315; AlH_6K_2Li-245317; AlH_6K_3-153683; AlH_6K_3-153684; AlH_6La-247037; AlH_6Li_3-99217; AlH_6Nd-247043; AlH_6Pr-247041; $AlHf_2$-150773; AlI_2Pd_5-14164; AlI_4Na-400521; AlI_8P-35403; $AlKO_2$-88774; $AlKSb_4$-300157; $AlKTe_2$-44703; $AlLaO_3$-28629; $AlLi$-240114; $AlLiO_2P_4$-74860; $AlLiO_2$-23815; $AlLiO_2$-28288; $AlLiO_4Si$-97909; $AlLiS_2$-608360; $AlLiSe_2$-280225; $AlLiTe_2$-162672; $AlLiTe_2$-280226; $AlLi_3N_2$-25565; $AlLi_5O_4$-1037; $AlLi_5O_4$-16229; $AlLuO_3$-0000; $AlMgSi$-153548; $AlMoO_7V$-280775; $AlMo_4S_8$-36564; $AlNNd_2O_3$-201358; $AlNaO_2$-22216; $AlNaO_2$-79404; $AlNaSe_2$-44704; $AlNaTe_2$-44701; $AlNdO_3$-10333; $AlNdPd_2$-604244; $AlNdPt$-150174; AlO_3Pr-35549; AlO_3Y-167509; AlO_4P-24511; AlO_4P-72374; AlO_4RbSi-160823; AlO_4V_2-151457; $AlPS_4$-15910; $AlPd$-58112; $AlPdTb$-54938; $AlPdYb$-370028; $AlPd_2$-58115; $AlPd_2Pr$-604243; $AlPd_5$-245328; $AlPrPt$-150173; $AlPtY$-609165; $AlPt_2$-459; $AlRe_2$-58147; $AlSe_2Tl$-100130; $AlSiSm$-151717; $AlSm$-609374; $AlTb$-58172; $AlTc_2$-609480; AlY_2-58211; $AlZr_2$-150774; Al_2Pd_8-58119; Al_2Pt_8-58136; $Al_2B_2BaO_7$-409171; $Al_2B_2CaO_7$-86785; $Al_2B_2O_7Sr$-89423; Al_2BaGe_2-98514; Al_2BaGe_2-98515; $Al_2BaO_7Sb_2$-154362; Al_2BaSi_2-249559; $Al_2Ba_3F_2$-413546; $Al_2Ba_3N_4$-410578; $Al_2Ba_3O_2Si_3$-27386; Al_2BeO_4-34806; $Al_2Be_2Cl_2Na_8O_{24}Si_8$-55253; $Al_2Bi_6Ca_5$-36364; Al_2Br_8Ti-39243; $Al_2C_3Th_2$-81572; Al_2CaCl_8-56730; Al_2CaGa_2-300209; $Al_2CaH_4O_8Si$-100320; Al_2CaH_8-246482; Al_2CaZn_2-57550; $Al_2Ca_2O_9Sn_2$-260890; $Al_2Ca_3F_4Na_2$-202657; $Al_2Ca_3Ge_3$-31982; $Al_2Ca_3H_2O_2$-15379; $Al_2Ca_3N_4$-280348; $Al_2Ca_3O_2Si_3$-16750; $Al_2Ca_5Sb_6$-60146; Al_2CdS_4-25634; Al_2CdSe_4-25637; Al_2CdTe_4-25640; Al_2CeGa_2-55789; Al_2CeZn_2-57594; Al_2CeZn_2-606526; $Al_2Cl_8Te_4$-10322; Al_2Cl_8Yb-56729; Al_2Cu-42517; Al_2CuU-23257; Al_2CuYb-604213; $Al_2Dy_3Ni_6$-105027; $Al_2Er_3Ni_6$-107804; $Al_2F_2Li_3Na_3$-9923; $Al_2FK_4NbO_{20}$-65738; $Al_2F_2GeO_4$-409714; Al_2FeS_4-607619; $Al_2Fe_3O_2Si_3$-28030; Al_2Ga_2La-607781; Al_2Ga_2Pr-607795; Al_2Ga_2Yb-607817; $Al_2Gd_2O_7Sr$-33580; Al_2Ge_8Sc-76361; Al_2HgS_4-25635; Al_2HgSe_4-25638; Al_2HgTe_4-25641; $Al_2Ho_3Ni_6$-105154; Al_2LaZn_2-105503; $Al_2La_5Ru_3$-167948; Al_2MgS_4-107308; Al_2MgS_4-38344; Al_2MgS_4-608441; Al_2MgSe_4-41926; $Al_2Mg_3O_2Si_3$-15438; Al_2MnS_4-608507; Al_2MnTe_4-608538; $Al_2N_2O_3SiSr$-408170; $Al_2N_4Sr_3$-74824; $Al_2Ni_6Y_3$-105538; $Al_2O_2P_3Tl_3$-280212; $Al_2O_2S_3$-32589; $Al_2O_2Si_3Sr_3$-27385; $Al_2O_2W_3$-73878; Al_2O_3-84375; Al_2O_3-9770; Al_2O_5Si-24275; $Al_2O_9Pb_2Si_2$-159977; Al_2Os-58108; Al_2Pb_2Sr-25336; Al_2Pd_5Pu-166270; Al_2Pd_5U-161313; Al_2Pd_5U-168816; Al_2Pd_5Y-182835; Al_2PrZn_2-106244; Al_2Ru-609234; Al_2S_4Zn-609280; $Al_2Sb_6Sr_5$-62304; $Al_2Sb_6Yb_5$-409996; Al_2Se_4Zn-25636; Al_2SmZn_2-609398; Al_2Te_4Zn-25639; Al_2Ti-107009; $Al_{30}Mg_{23}$-57965; Al_3AuCe-658144; Al_3Au_8-57502; $Al_3B_4GdO_2$-100831; $Al_3B_4NdO_2$-6175; $Al_3B_4O_2Y$-20223; $Al_3Bi_5Cl_2$-201993; $Al_3Ca_2HO_3Si_3$-9245; Al_3Ca_4Mg-152756; $Al_3Cs_2F_2Na$-646; Al_3CuGd-658383; $Al_3Er_5Ge_4Ni_3$-172068; $Al_3F_9Pb_5$-203224; Al_3FeSi_2-79710; Al_3Gd-607838; $Al_3H_6KO_4S_2$-12106; Al_3Hf-109214; Al_3Ho-150555; Al_3ITe_3-66030; $Al_3Li_2Si_4$-39597; Al_3Nb-58015; Al_3NiY-160931; $Al_3O_2Sc_2Y_3$-67055; Al_3Os_2-58109; Al_3Pd_5-58118; Al_3Ru_2-609226; Al_3Sc-247449; Al_3Ta-58169; Al_3Tb-150557; Al_3Ti-58189; Al_3V-58201; Al_3Y-58217; Al_3Zr-106259; Al_3Zr_5-603491; $Al_4AuErGe_2$-415290; Al_4Ba-606140; Al_4BaS_7-33237; $Al_4Ba_6F_{24}$-37034; $Al_4Bi_2O_9$-20069; $Al_4Bi_4Cl_6Se_4$-414155; $Al_4Bi_4Cl_6Te_4$-411714; $Al_4Br_4La_5$-413559; Al_4C_3-14397; Al_4C_4Th-81573; $Al_4C_5Hf_2$-161586; $Al_4C_5Zr_2$-173676; $Al_4C_6Hf_3$-161585; $Al_4C_6Zr_3$-173677; Al_4Ca-151189; Al_4Ce-57556; Al_4CeCo-55598; Al_4CoLa-9986; Al_4CoNd-154678; Al_4CoPr-600912; Al_4ErMo_2-607414; Al_4Eu-55427; Al_4Fe_8U-607702; $Al_4Ge_2NiTb_2$-95799; Al_4La-

57935; Al_4Mo_2Yb-456; Al_4Nd-150508; Al_4Ni_3-58042; Al_4Pr-150507; Al_4Sm-609379; Al_4Sr-107887; $Al_5Br_4La_0$-409704; Al_5CePt_3-171199; $Al_5Er_3O_2$-62615; $Al_5Gd_3O_2$-23849; $Al_5Ho_3O_2$-33603; $Al_5Lu_3O_2$-23846; $Al_5NaO_2Ti_2$-15346; Al_5Ni_2Zr-58084; $Al_5O_2Tb_3$-33602; $Al_5O_2Y_3$-16825; $Al_6AuDy_2Si_4$-281661; $Al_6AuSi_4Tb_2$-281659; $Al_6C_3N_2$-14399; $Al_6Ca_0Ge_9$-417966; $Al_6Ca_4O_3$-16177; $Al_6Ca_4O_6W$-28481; $Al_6Dy_2PtSi_4$-281660; Al_6OSr_2-97713; $Al_6O_6SSr_4$-28482; $Al_6O_6Sr_4W$-28483; $Al_6PtSi_4Tb_2$-281658; Al_7Au_3Ce-391101; Al_7Au_3Dy-391108; Al_7Au_3Er-391109; Al_7Au_3Gd-391102; Al_7Au_3Ho-391106; Al_7Au_3Lu-391105; Al_7Au_3Nd-391107; Al_7Au_3Pr-391104; Al_7Au_3Tb-391103; $Al_7Ca_3Cu_2$-57538; Al_7Te_0-62659; Al_7Th_2-58186; $Al_8C_3N_4$-14401; Al_8CaCo_2-57533; Al_8CaCu_4-57539; Al_8CaFe_4-606314; Al_8CaMn_4-57545; Al_8CeCr_4-606419; Al_8CeCu_4-57566; Al_8CeFe_4-57574; Al_8CeMn_4-57579; Al_8Co_2Pr-600914; Al_8Co_2Sm-600915; Al_8Cr_4Dy-606767; Al_8Cr_4Er-606769; Al_8Cr_4Gd-156967; Al_8Cr_4Ho-606790; Al_8Cr_4La-606792; Al_8Cr_4Nd-606817; Al_8Cr_4Pr-606830; Al_8Cr_4Tb-606848; Al_8Cr_4Y-57664; Al_8Cr_4Yb-606871; Al_8Cr_5-606753; Al_8Cu_4Dy-606899; Al_8Cu_4Er-606913; Al_8Cu_4Gd-606934; Al_8Cu_4Ho-606964; Al_8Cu_4Nd-607039; Al_8Cu_4Pr-607058; Al_8Cu_4Tb-607133; Al_8Cu_4Th-607143; Al_8Cu_4U-57724; Al_8Cu_4Y-57727; Al_8Cu_4Yb-607191; Al_8DyFe_4-57749; Al_8DyMn_4-607312; Al_8ErFe_4-607382; Al_8ErMn_4-607409; Al_8ErMn_4-607412; Al_8EuMn_4-607460; Al_8Fe_4Gd-607505; Al_8Fe_4Hf-607535; Al_8Fe_4Ho-57752; Al_8Fe_4La-607554; Al_8Fe_4Nd-607593; Al_8Fe_4Sc-164856; Al_8Fe_4Tb-57823; Al_8Fe_4Th-54990; Al_8Fe_4U-54991; Al_8Fe_4Y-57842; Al_8Fe_4Yb-607748; Al_8Fe_4Zr-607756; Al_8Fe_5-169545; Al_8Fe_5-169547; $Al_8Ge_3Sr_4$-173215; Al_8HoMn_4-608195; Al_8LaMn_4-608299; Al_8LuMn_4-608379; Al_8Mn_4Nd-608479; Al_8Mn_4Pr-608494; Al_8Mn_4Sc-99142; Al_8Mn_4Tb-608537; Al_8Mn_4U-608550; Al_8Mn_4Y-57997; Al_8Mn_4Yb-608570; Al_9ErNi_3-105031; Al_9Sr_5-655752; $AsRb_3$-412872; As_2Fe_4La-168584; As_2Fe_4La-23080; $As_2Ni_2Re_5$-35731; $AsBO_4$-26891; $AsBO_4$-413436; $AsBO_4$-413438; AsB_6-68151; $AsBeCsO_4$-74027; $AsBiCu_2O_6$-88111; $AsBiO_4$-30636; $AsBi_3Ni_8S_6$-203066; AsC_3H_0I-171203; $AsCaCoHO_5$-240725; $AsCaHNiO_5$-202422; $AsCaHO_5Zn$-63285; AsCaPt-60828; $AsCa_2$-166865; $AsCa_2ClO_4$-26234; $AsCa_2I$-65218; $AsCa_3N$-657354; AsCd-432; AsCdNa-9571; $AsCd_3Cl_3$-23306; $AsCeFO_4$-166934; AsCeRh-90869; $AsClO_2Pb$-66246; $AsCl_3$-280796; $AsCl_3F_6S$-60076; $AsCl_5$-412103; AsCo-15065; AsCoHf-406953; AsCoRh-43896; AsCoS-31189; AsCoSe-41731; AsCr-23589; $AsCrO_4$-62132; $AsCr_3N$-25760; $AsCsF_6$-408070; $AsCsO_5Ti$-280315; $AsCsSe_2$-65299; $AsCs_3O_4$-412392; $AsCs_3Se_4$-404082; $AsCuHO_5Zn$-160894; AsCuMg-412296; AsCuMn-72413; AsCuS-23826; $AsCuSe_2$-42884; $AsCu_3$-655109; $AsCu_3S_4$-14285; $AsCu_3Se_4$-610361; $AsDyO_4$-16512; AsErPd-409908; $AsEuO_4$-409995; AsEuPt-60829; AsF_3-35132; AsF_5-65477; $AsF_5H_6N_2$-412507; AsF_6In-417952; AsF_6K-38130; AsF_6Li-74831; AsF_6Na-184563; AsF_6Na-184565; AsF_6Rb-408069; AsF_6Tl-417954; AsF_7Sn-816; AsF_9OS-10193; AsFe-15009; AsFeLi-187132; $AsFeLiO_4$-245182; AsFeS-15986; AsFeTa-610528; AsGa-43951; $AsGa_2Rh_5$-56973; AsGeSe-100828; $AsHHgO_5Zn$-281591; $AsHO_5PbZn$-98385; $AsHO_5Zn_2$-34868; AsH_2LiO_4-62024; AsH_2LiO_5Zn-409396; $AsH_{36}Li_3N_2Se_4$-409539; AsH_4NaO_5-4284; AsH_6NO_4-28155; AsH_6NO_4-66208; $AsHf_2$-610638; $AsHoO_4$-155919; AsHoPd-71619; AsI_3-23003; AsI_3La_3-411803; AsI_3S_{24}-412399; $AsKLi_2$-78938; $AsKMoO_6$-203218; $AsKNiO_4$-63544; $AsKO_2$-413149; $AsKS_5Sn$-281038; AsLaRh-95191; AsLaTe-280231; $AsLiMgO_4$-67523; $AsLiMnO_4$-245181; $AsLiMoO_6$-15035; $AsLiNiO_4$-51201; $AsLiO_3$-202862; $AsLiO_5Ti$-78105; $AsLiO_5V$-90991; $AsLi_2NaO_4$-73200; $AsLi_3O_4$-75927; $AsLi_3S_3$-59381; $AsLuO_4$-2506; AsMn-9496; $AsMnNaO_4$-95087; AsMo-43188; $AsNaNiO_4$-63353; $AsNaO_2$-16762; AsNb-

16585; AsNiTa-611079; $AsNi_2Si$-83753; AsO_2Rb-413150; AsO_4P-31879; AsO_4Sc-155920; AsO_4Tb-16329; AsO_4Y-24513; AsO_5RbSn-80977; AsO_5RbTi-71907; AsO_5Sb-36650; AsPdZr-92440; AsRb-412594; $AsRb_3Se_4$-404080; AsRh-42572; AsRhTi-44052; AsRhV-107965; $AsRh_2$-611266; AsRu-42577; AsSSm-96227; AsS_3Tl_3-100292; AsS_3Tl_3-79580; $AsSe_3Tl_3$-15148; AsTa-44068; $AsTa_2$-611452; AsTeU-42366; AsTiZr-92989; AsV-42445; AsZn-431; As_2BaCo_2-609848; $As_2BaCo_2O_8$-260062; As_2BaCr_2-609849; As_2BaCu_2-236307; As_2BaCu_4-89628; As_2BaFe_2-166018; As_2BaMn_2-41794; As_2BaNi_2-164197; As_2BaNi_2-609856; $As_2BaNi_2O_8$-27014; As_2BaPd_2-36377; As_2BaRh_2-165121; As_2BaRu_2-165119; As_2BaZn_2-12146; As_2BaZn_2-417000; $As_2Ba_2MnO_2Zn_2$-85659; $As_2Ba_2Mn_3O_2$-32011; $As_2Ba_2O_2Zn_3$-67998; $As_2Ba_3O_8$-404438; As_2Ba_4O-33905; As_2BeK_4-300111; $As_2Br_2Cd_2Hg_2$-240354; As_2CaCo_2-609899; As_2CaCu_4-32619; As_2CaFe_2-166016; As_2CaGa_2-422526; As_2CaNi_2-23004; As_2CaPd_2-36372; As_2CaRu_2-602108; As_2Ca_4O-68203; As_2Cd-16037; As_2CdGe-16736; As_2CdK_4-300190; As_2CdSi-22187; As_2CdSn-16737; As_2CeCo_2-610002; As_2CeNi_2-68146; As_2CePd_2-604354; $As_2Cl_3Hg_3Tl$-411520; As_2Co-610034; As_2Co_2K-610072; As_2Co_2La-610073; As_2Co_2Nd-610090; As_2Co_2Pr-610099; As_2Co_2Sr-610122; As_2CsRh_2-610296; As_2CsRu_2-610297; As_2Cu_2Sr-78756; $As_2Cu_3K_3$-32015; As_2Cu_4Eu-89627; As_2Cu_4K-59207; As_2Cu_4Sr-89626; As_2EuFe_2-163211; As_2EuNi_2-610437; As_2EuPd_2-604348; As_2EuRh_2-416982; As_2Eu_4O-1222; As_2F_2Mn-83635; $As_2F_6MgXe_2$-281694; $As_2F_2OSr_2Ti_2$-167013; As_2Fe-41724; As_2Fe_2Rb-167329; As_2Fe_2Sr-163209; As_2GdNi_2-610591; As_2Ge-610599; As_2GeMg-182368; As_2GeTe_4-68111; As_2GeZn-16735; $As_2Ge_3Te_6$-68113; As_2Hf_3-610637; As_2HgK_4-402573; $As_2Hg_4O_7$-391228; $As_2K_3NbO_9$-202980; As_2K_4Zn-409919; As_2LaNi_2-68145; As_2LaPd_2-604343; As_2LaRu_2-602111; As_2MgSi-182367; As_2Mg_3-610828; $As_2Mn_3O_2Sr_2$-32010; As_2NaSn_2-82366; As_2NbNi-38412; As_2NdNi_2-611001; As_2NdPd_2-604337; As_2Ni-24204; As_2Ni_2Pr-611047; As_2Ni_2Sr-23005; As_2OW_2-15020; As_2OSr_4-33904; As_2OYb_4-402951; As_2O_4-10436; As_2O_5-987; As_2O_6S-32581; $As_2O_6Zn_3$-10400; $As_2O_8Sr_3$-420295; As_2Os-995; As_2Pd_2Pr-604345; As_2Pd_2Sm-604347; As_2Pd_2Sr-36374; As_2Rh_2Sr-165120; As_2Ru-994; As_2Sc_3-16411; As_2SiZn-22184; As_2SnZn-18203; As_2Sn_2Sr-611428; As_2Sn_2Sr-82371; As_2Ti-20488; As_2Zr-168665; As_2Zr_3-611611; As_3Ba_3In-402338; As_3Ba_3NbO-408853; As_3Ba_3OTa-280155; As_3CaFe_4-260320; As_3Ca_3Ga-60126; As_3Cd_4K-262032; As_3Cd_4Rb-262037; As_3Ce_4-43883; As_3Co-655090; As_3CoHf_5-85884; $As_3Cr_2Na_3O_2$-280946; As_3Cs_5Ge-65718; As_3Cs_5Si-65716; As_3Eu_4-610400; As_3Ir-34046; $As_3K_5O_0$-23302; As_3LaSi-39160; As_3La_4-610771; $As_3Mg_4NaO_2$-59888; $As_3NaO_2Ti_2$-421531; $As_3NaO_2Zr_2$-97956; As_3NaZn_4-262036; As_3Nb_5-16417; As_3OSr_3Ta-409567; As_3Pr_4-611220; As_3Rb_5Si-300191; As_3Rh-34052; As_3Sn_4-419884; As_3Sr_4-402110; As_3Ti_4-611492; As_3Ti_5-611496; As_3V_5-611571; As_3Yb_4-611589; As_3Yb_4-95562; As_4BaCu_8-66017; $As_4Ca_3In_2$-61336; As_4Cd_2Ge-42132; As_4ClCuS_3-419754; As_4CsF_3-281641; $As_4Cu_2S_2$-33588; $As_4Cu_2S_3$-26724; $As_4Cu_6Hg_3S_2$-200785; $As_4Cu_6Hg_3S_2$-20424; $As_4Eu_3Pd_4$-79094; As_4K_7Nb-380109; As_4K_7Ta-380110; As_4Mo_5-43186; As_4NbRb_7-380111; $As_4Nb_5Pd_4$-412866; As_4Pa_3-611159; $As_4Pb_9S_5$-18097; $As_4Rb_5TaTl_2$-85784; As_4S_3-16105; As_4Ta_5-36525; As_4Th_3-611490; As_4U_3-611550; $As_5Cu_4U_2$-69726; $As_5K_6Sn_3$-71009; $As_6Ca_5Ga_2$-27; $As_6Ca_5Sn_2$-61037; $As_6Cu_7Se_3$-15235; $As_6Ir_7Mg_4$-94393; $As_6Mg_4Rh_7$-94391; $As_6Rh_7Yb_4$-94392; $As_6Ru_7U_4$-90326; As_7Re_3-26270; As_7Re_3-611260; AuBa-419559; $AuBa_2Tl_7$-98964; $AuBa_4C_4KO_4$-40854; $AuBa_4NaO_8$-73189; $AuBe_2$-109312; AuBr-200286; AuBrSe-2897; AuC_2KN_2-26498; $AuC_4H_2KN_4O$-16043; AuCaCd-420574; AuCaGa-106273; AuCaIn-408579; $AuCa_3$-58401; AuCd-58409; AuCdEu-

411544; AuCdYb-411545; AuCe-611711; $AuCeCu_5$-107971; AuCeZn-418712; $AuCe_2P_3$-411550; AuCl-6052; $AuClF_3P$-415842; AuClO-8190; $AuCsK_2O_2$-62064; AuCsO-409553; AuCsO-43006; AuCsTe-71653; $AuCs_3Ge_4$-413725; $AuCs_3Pb_4$-107448; AuEu-611844; AuEuZn-420674; $AuFTh_2$-89619; $AuFU_2$-152058; AuF_3-80478; AuF_4K-10327; AuF_4K-9906; AuF_4Na-9905; AuF_4Rb-9907; AuF_6K-415874; AuF_6Li-165209; AuGa-58457; AuGeYb-85835; $AuGe_4K_3$-413728; $AuGe_4Rb_3$-413724; $AuHf_2$-58471; $AuHo_2$-58480; $AuI_2K_5O_2$-40376; AuInSr-391422; $AuKNa_2O_2$-61226; $AuKO_2$-15115; AuK_3Se_2-402000; AuK_3Sn_4-107444; AuLa-612101; $AuLaO_3$-73873; $AuLa_2$-612100; $AuLi_2Sn_2$-55349; AuMgYb-411303; $AuMg_2$-58540; $AuMn_2$-58548; AuN_2-166465; AuNaSn-58554; AuNaSn-660108; $AuNa_2$-58527; $AuNa_2O_2Rb$-411460; $AuNa_3S_2$-202329; AuNd-612217; $AuNi_2Sn_4$-150127; AuORb-409552; $AuPb_2$-150949; $AuPb_2$-56272; $AuPb_3$-58567; $AuPb_4Rb_3$-107447; AuPr-612264; AuRbTe-71652; $AuRb_2S_4Sb$-54507; $AuRb_3Sn_4$-107445; AuSbTl-391381; $AuSb_3$-43504; AuSm-612335; AuSnSr-412013; $AuSn_2$-58587; $AuTe_2$-38213; $AuTh_2$-150644; AuTi-612407; $AuTl_2$-102798; AuYb-612473; AuYbZn-159306; $AuYb_2$-58619; $AuZr_2$-108025; $AuZr_2$-612511; Au_2BaF_2-39316; Au_2BaF_8-65289; Au_2BaIn_2-249562; Au_2BaO_4-80327; Au_2Be-150581; Au_2BiDy_5-156957; Au_2BiEr_5-156959; Au_2BiHo_5-156958; Au_2BiTb_5-156956; $Au_2Br_2H_2N_4$-80216; $Au_2Br_6Cs_2$-170696; Au_2CaGe_2-25333; Au_2CaO_4-79801; Au_2CaSi_2-412; $Au_2Cd_2Rb_2S_4$-85582; Au_2CeGe_2-246610; Au_2CeSi_2-58424; $Au_2Cl_6Cs_2$-6061; $Au_2Cs_2I_6$-59269; Au_2Dy-58440; Au_2Dy-611781; Au_2In_2Sr-249563; $Au_2La_4O_9$-74989; $Au_2O_7Se_2$-37009; Au_2Sr_3-58596; $Au_3Ca_2In_4$-410702; Au_3Dy-611784; Au_3Er-611810; Au_3EuIn_3-245680; Au_3F_2La-78915; Au_3Hf-611955; Au_3Ho-58482; Au_3In-612016; Au_3In_3Sr-245679; Au_3KSn_3-249645; $Au_3K_3Sb_2$-78977; $Au_3La_3Sb_4$-612105; Au_3Lu-612128; $Au_3O_2Rb_5$-91308; $Au_3Pr_3Sb_4$-612269; Au_3Rb_2Tl-249924; $Au_3Rb_3Sb_2$-78978; $Au_3Sb_4Y_3$-957; Au_3Sm-58585; $Au_3Sn_2Yb_2$-710044; $Au_3Sn_4U_3$-612361; Au_3Tb-612380; Au_3Y-612464; Au_3Yb-58620; Au_3Zr-612509; Au_4Ca_3-54547; Au_4Hf-611961; Au_4Li_5-150973; $Au_4S_3Tl_2$-51235; Au_4Th_3-601382; $Au_7Cs_4Sn_2$-107449; $Au_7Ge_2K_4$-79111; $Au_7Rb_4Sn_2$-58581; BLi-164842; $B_2Ba_7Ir_2$-8156; $B_2BrCs_3H_2$-414584; $B_2BrH_2K_3$-2120; $B_2BrH_2Rb_3$-414583; $B_2Cs_3H_2I$-98622; $B_2H_2IK_3$-98619; $B_2H_2IRb_3$-98620; $B_2O_{24}Se_2Zn_8$-74057; B_2P_2-62748; B_2Si_3-615435; B_3C_2-446; $B_6Ir_9Mg_0$-163909; BBa_2ClN_2-418947; BBe_2FO_3-56847; $BBe_2F_2KO_3$-77277; $BBe_2F_2O_3Rb$-164854; $BBrEu_2N_2$-409982; $BBrN_2Sr_2$-261795; $BCF_4H_6N_3$-202434; BC_3H_2N-249799; BC_7-181956; $BCrO_3$-43311; BF_3-24783; BF_4Li-171375; BF_5Li_2-426821; $BFeO_3$-34474; $BH_0Li_4N_3$-171352; BI_2Zr_6-202103; $BInO_3$-75254; BLi_3N_2-155128; BLi_3O_3-9105; $BLuO_3$-16525; $BNaO_2$-34645; BO_3Sc-65010; BO_3Ti-402039; BO_3V-45060; BO_3Yb-160141; BS_2Tl-71593; B_2BaO_6Ti-97972; B_2BaO_6Zr-95527; $B_2Ba_2MgO_6$-75986; B_2CCe-40164; B_2CN-183792; B_2CTh-68414; B_2CU-44142; B_2CaO_6Sn-30998; $B_2Ca_3Ni_7$-36505; $B_2Ca_3O_6$-1894; $B_2Ce_2Ir_5$-97343; B_2Co_3Zr-16179; $B_2Eu_3O_6$-86479; B_2F_4-27867; B_2H_8KNa-163377; $B_2Hg_3O_6$-71261; $B_2K_2O_6Zr$-67982; B_2Li_2-1; B_2MgO_6Sn-28266; B_2Mo-40907; B_2O_6SnSr-28267; $B_2O_6Sr_3$-93395; $B_3Ba_4N_6Na$-401210; $B_3Ca_4LiN_6$-400339; $B_3Eu_4LiN_6$-400465; $B_3H_3O_4Zn_8$-416894; $B_3LiN_6Sr_4$-402173; B_3Mo-167734; $B_3N_6NaSr_4$-92577; $B_3Na_3O_6$-15967; $B_3Na_3O_9Sc_2$-245063; $B_3Na_3S_6$-79613; $B_3O_6Rb_3$-59826; $B_3O_9ScSr_3$-75339; $B_3Rb_3S_6$-79615; B_4C-29093; $B_4CeO_2Sc_3$-90839; $B_4Fe_3LaO_2$-83506; $B_4Fe_3NdO_2$-83507; $B_4Fe_3O_2Tb$-96455; $B_4Ga_3NdO_2$-200321; $B_4LaO_2Sc_3$-89013; B_4Mo_2-39554; B_5W_2-20326; B_6BaNi_2-100287; $B_6Ba_2CaO_2$-30890; $B_6Ba_2MnO_2$-391013; $B_6Ba_2Ni_9$-100288; $B_6BrK_3O_0$-172400; B_6CaNi_2-36507; $B_6Co_4O_3$-96561; B_6EuNi_2-86371; B_6Ni_2Sr-100286; B_6O-71065; $B_6O_3Zn_4$-100290; $B_6O_8ScSr_6Y$-67648; $B_7ClCo_3O_3$-

158297; $B_7ClO_3Zn_3$-55444; B_9BaLiO_5-93013; B_9BaNaO_5-93014; B_9MgN-280938; $Ba_2Li_8N_6Na_5$-417928; $BaBiO_3$-151895; $BaCN_2$-75041; $BaCO_3$-158389; BaC_2CeFO_6-74178; $BaC_2F_2O_6Pb_2$-280899; BaC_2MgO_6-24435; $BaCeO_3$-79627; $BaCrF_6$-10341; $BaCu_2Ga$-615828; BaF_2-183923; BaF_2-41649; BaF_2-41650; BaF_3Li-45310; BaF_4Pd-108991; BaF_6Ge-26614; BaF_6Ni-35396; BaF_6Pb-25521; BaF_6Rh-6038; BaF_6Si-26613; BaF_6Sn-33788; BaF_6Ti-33789; BaF_7Ta-417251; $BaFeO_3$-28917; $BaGe_2Pt_4$-174551; $BaGe_2Li_2Mg_2$-409576; BaH_9Re-247108; BaH_9Re-247109; $BaHgO_2$-74076; $BaLi_2Mg_2Si_2$-409575; $BaMnO_3$-66822; $BaMn_3O_{38}Ti_8$-81584; $BaMo_2O_2P_3$-68560; $BaMo_6S_8$-615980; $BaMo_6S_8$-62157; $BaNb_2OV_2$-165097; $BaNi_2O_8P_2$-280167; $BaNi_2O_8V_2$-96086; $BaNi_4O_8$-20898; BaO_8V_3-51472; BaO_3Ru-10253; BaO_3Si-156705; BaO_3Tb-2752; BaO_3Ti-6102; $BaPb_3$-419973; $BaRu_4Sb_2$-42963; Ba_2BiIrO_6-174290; Ba_2BiO_6Sb-172761; Ba_2BiO_6Ta-153120; Ba_2BiO_6Yb-80902; $Ba_2Bi_2O_6$-28164; Ba_2BrCuO_2-67395; Ba_2BrN-262056; $Ba_2C_3Cs_2O_9$-73170; $Ba_2ClCo_4O_7$-245991; Ba_2ClCuO_2-1038; Ba_2ClN-262051; Ba_2ClP-28134; Ba_2CoF_6-21057; $Ba_2Cr_7O_4$-2766; Ba_2FN-262049; Ba_2F_6Ni-21056; Ba_2F_6Zn-21054; Ba_2HN-67510; Ba_2IrLaO_6-152678; Ba_2IrO_6Sr-74030; $Ba_2Ir_3O_9$-54725; Ba_2LaO_6Ru-155549; Ba_2LaO_6Sb-153136; Ba_2LaO_6Ta-160170; $Ba_2La_2MnO_2W_2$-54667; Ba_2Mg_7-58660; $Ba_2Nb_5O_{32}$-69991; Ba_2NbO_6Pr-245457; Ba_2NiO_6Te-25005; Ba_2O_6PrSb-153137; Ba_2O_6SrTe-246109; Ba_2O_6SrTe-246109; Ba_2O_6SrW-246114; Ba_2Re_6S-30737; $Ba_3BeCl_8Zr_6$-33993; Ba_3BiNaO_6-72839; $Ba_3Cl_2Fe_2O_5$-48178; $Ba_3Cr_2O_8$-9457; $Ba_3Cr_2S_6$-97540; $Ba_3Dy_4O_9$-72480; $Ba_3Er_4O_9$-72481; $Ba_3Ho_4O_9$-33807; Ba_3IrNaO_6-405134; $Ba_3Lu_4O_9$-38383; $Ba_3Mn_2O_8$-280045; Ba_3NaNbO_6-72330; Ba_3NaO_6Ru-405133; Ba_3NaO_6Ta-72331; $Ba_3Nb_2O_8$-95193; Ba_3NiO_4-30662; $Ba_3O_8P_2$-18110; $Ba_3O_8P_2$-30634; $Ba_3O_8V_2$-14237; $Ba_3O_9W_2$-100689; $Ba_3O_9Y_4$-87118; $Ba_4CeMn_3O_2$-99661; $Ba_4ClO_8Os_6$-82910; $Ba_4ErO_2Ru_3$-174186; $Ba_4HoO_2Ru_3$-160868; $Ba_4Mn_3NdO_2$-156305; $Ba_4Mn_3O_2Pr$-99662; $Ba_4NaO_2Sb_3$-160173; $Ba_4O_2Ru_3Tb$-160870; $Ba_4O_2Ru_3Zr$-47132; Ba_4O_6Pt-65706; Ba_6NNa_6-78394; $Ba_6N_6OOs_2$-419467; $Ba_6N_6ORe_2$-419636; $Ba_6O_8W_4$-9725; $Ba_9O_{24}Sc_2Si_6$-75175; Be_7Nb_2-58724; Be_7Ru_3-58735; Be_7Ti_2-109217; Be_7Zr_2-58759; $BeCl_2$-173561; $BeCsF_3$-290357; BeF_2-173557; BeF_2-173558; BeF_2-9481; BeF_4Li_2-14360; BeK_4P_2-300110; Be_2CsF_5-2801; $Be_2F_8K_2Pb$-9902; $Be_2F_8K_2Sr$-109005; Be_2O_4Si-28003; $Be_3Ca_3F_2Li_2O_2Si_3$-39389; Be_3Nb-58723; Be_3Ru_2-616409; $Be_4C_6K_6O_9$-412642; Bi_2GeO_{20}-39611; Bi_2MnO_{20}-75079; $Bi_2O_{20}Si$-422389; $Bi_2O_{20}Ti$-167355; $Bi_2O_{20}Zn$-62479; $BiCsF_6$-15122; BiF_3-25567; BiF_3-655136; BiF_3-9015; BiF_4K-63166; BiF_4Li-65404; BiF_5-25023; BiF_6K-25024; BiF_6Li-15119; BiF_6Na-15120; BiF_6Rb-15121; $BiFeO_3$-15299; BiK_3O_3-407293; $BiNa_3O_3$-23347; $Bi_{24}Ge_2O_{40}$-68431; $Bi_{24}Mn_2O_{40}$-75390; $Bi_{24}O_{40}Pb_2$-75392; $Bi_{24}O_{40}Si_2$-68430; $Bi_{24}O_{40}Ti_2$-75389; $Bi_2Ni_3S_2$-159364; $Bi_2Pd_3S_2$-417634; Bi_3Eu_4-616649; Bi_3Gd_4-616662; Bi_3La_4-616755; Bi_3Nd_4-616855; Bi_3Nd_4-616860; Bi_3Sm_4-617132; Bi_3Tb_4-617161; Bi_3Yb_4-617255; $Bi_4Ce_3Pd_3$-419162; $Bi_4Cu_3La_3$-167250; $Bi_4Ge_3O_2$-260560; $Bi_4O_2Si_3$-402349; Bi_4Rh-58854; Bi_4Th_3-617222; Bi_4U_3-617239; Br_5CoTh_6-33926; Br_5FeTh_6-33925; BrF_3-31689; BrF_4K-10326; BrF_4Rb-65713; BrF_5-31690; $Br_2Cs_2F_2$-84021; $Br_2Cs_2F_2$-84022; $Br_2Hg_3Te_2$-27402; Br_3La_3Si-411800; $C_2Cl_2N_2O_4P_4S_2Sb_4$-80097; $C_2O_2Ru_4Se_4$-92913; $C_8Er_0Mn_3$-603261; $C_8Ho_0Mn_3$-603286; $C_8Lu_0Mn_3$-603277; $C_8Mn_3Tb_0$-603285; C_8Ru_2Th-79240; CCl_3Gd_3-37323; CF_4-2848; CF_4-66659; CLi_2O_3-66942; CLi_2O_3-96486; $C_{22}F_4$-411879; C_3Ce_2-74661; $C_3Cs_2O_9Sr_2$-169231; C_3Dy_2-2449; C_3Er_2-86291; C_3F_6-151184; C_3Gd_2-602774; C_3Ho_2-42497; C_3La_2-618154; C_3Lu_2-618221; C_3N_4-97565; C_3Nd_2-2447; $C_3O_9Rb_2Sr_2$-169232; C_3Pr_2-74662; C_3Pu_2-24620; C_3Sc_4-42760; C_3Tb_2-74663; C_3Tm_2-86292; C_3U_2-618999; C_3Yb_2-86293;

$C_{60}Eu_6$-88616; $C_{60}K_6$-66879; $Ca_2Li_6N_6O_3Re_4$-411462; $CaCo_4Cu_3O_2$-169095; $CaCsF_3$-45309; $CaCs_2F_4$-82616; $CaCuF_4$-9928; $CaCu_3Ge_4O_2$-1303; $CaCu_3Mn_4O_2$-156374; $CaCu_3O_2Pt_4$-248230; $CaCu_3O_2Ru_4$-51894; $CaCu_3O_2Sn_4$-162100; $CaCu_3O_2Ti_4$-167254; $CaCu_3O_2V_4$-250094; CaF_2-44937; CaF_2-51237; CaF_2-51239; CaF_2-656449; CaF_3K-154074; CaF_3Rb-201253; CaF_4Pd-32674; CaF_4Zn-31366; CaF_6Pb-25522; CaF_6Sn-35713; $CaFe_3O_2Ti_4$-79277; $CaFe_4Sb_2$-42961; $CaNa_0Sn_2$-240006; CaO_3Si-240453; Ca_2F_4-246961; $Ca_2K_8O_{24}U_6$-91783; $Ca_3Cr_2O_2Si_3$-158537; $Ca_3Fe_2Ge_3O_2$-280047; $Ca_3Ga_2O_2Si_3$-27387; $Ca_3Ga_4Ni_4$-58899; $Ca_3Ge_3O_2Y_2$-280048; Ca_3Hg-58903; $Ca_3Ir_4Si_4$-95788; $Ca_3Mn_2O_2Si_3$-27388; Ca_3N_2-34678; $Ca_3O_2Sc_2Si_3$-27389; $Ca_3O_2Te_2Zn_3$-67045; $CdCsF_3$-290344; $CdCuF_4$-73478; $CdCu_3O_2Ti_4$-39467; CdF_2-183501; CdF_2-250165; CdF_3K-44788; CdF_3Rb-49587; Cd_2F_8Tb-86146; $Cd_3Ge_3O_2Sc_2$-20216; Cd_3N_2-416908; Cd_3P_2-620218; $Cd_4N_2P_6S$-71019; CeF_3-16965; CeF_3-4; CeF_3-42470; $CeFe_4P_2$-52852; CeP_2Ru_4-50595; $CeRu_4Sb_2$-621988; Ce_2O_3-96202; $Ce_3Cu_3Sb_4$-658638; $Ce_3Ni_6Si_2$-25622; $Ce_3Pt_3Sb_4$-621896; Ce_3S_4-31602; Ce_3Se_4-622113; Ce_3Te_4-43676; Ce_4Sb_3-52905; $Ce_6Ni_6P_7$-2243; $Ce_6P_7Pd_6$-30851; ClF-406442; ClF_3-19079; ClF_3Sn_2-2088; $Cl_2Hg_3Se_2$-27400; $Cl_2Hg_3Te_2$-27401; Cl_3F_2Sb-200039; Cl_3F_2Sb-380014; Cl_4CsLi_3-245975; Cl_4FSb-30629; Cl_4FTa-27413; Cl_4Li_2Zn-202743; Cl_8FeLi_6-73217; CoF_2-98785; CoF_3-16672; CoF_3-29133; CoF_3K-15246; CoF_4K_2-33522; CoF_4Rb_2-69683; CoF_6Rb_2-9701; CoF_6Zr-83724; CoP_3-624594; $CoSb_3$-41620; CoU-625521; $Co_2F_7K_3$-33524; Co_6Nd_2Sn-240094; $Co_7Ge_6Zr_4$-52996; $CrCs_2F_6$-29007; CrF_2-31827; CrF_3-59967; CrF_3K-172844; CrF_4-78778; CrF_4Sr-26105 (4); CrF_5-419661; CrF_6Nb-75384; CrF_6Rb_2-29006; CrF_6Zr-35719; $CrGa_4$-626026; Cr_2F_5-80639; $Cr_2Fe_3O_2Si_3$-27375; $Cr_2Mn_3O_2Si_3$-27379; $Cs_8O_6Tl_8$-421376; $CsCuF_4$-35264; $CsEuF_3$-49577; CsF-44288; CsF-53832; CsF-61563; CsF_2H-45858; CsF_2Li-18020; CsF_3Hg-15168; CsF_3Mg-290360; CsF_3Mg-49584; CsF_3Pb-290350; CsF_3Sr-49578; CsF_3Yb-49579; Cs_2CuF_6-65259; Cs_2F_4Hg-72353; Cs_2F_6Ge-35547; Cs_2F_6Mn-47201; Cs_2F_6Mn-76272; Cs_2F_6Si-26871; Cs_2F_6Si-38548; Cs_2O_3-627061; $Cs_3F_5Li_2$-245964; Cs_3F_6Tl-19076; Cs_3F_6Y-19078; $Cu_2S_3Sb_4$-25707; Cu_5Si_4-36254; CuF-52273; CuF_2-26576; CuF_2-9788; CuF_3K-21108; CuF_3Rb-69656; CuF_4K_2-15372; CuF_4K_2-24408; CuF_4Sr-9927; $Cu_2F_7K_3$-15373; $Cu_3DyMn_4O_2$-153871; $Cu_3Er_3Sb_4$-658645; $Cu_3GdMn_4O_2$-153870; $Cu_3Gd_3Sb_4$-658641; $Cu_3HoMn_4O_2$-153872; $Cu_3Ho_3Sb_4$-658644; $Cu_3LaO_2Ru_4$-51897; $Cu_3La_3Sb_4$-658637; $Cu_3Mn_4O_2Pr$-153867; $Cu_3Mn_4O_2Th$-34316; $Cu_3Mn_4O_2Tm$-153873; $Cu_3Mn_4O_2Y$-38419; $Cu_3Mn_4O_2Yb$-153874; $Cu_3NdO_2Ru_4$-51896; $Cu_3Nd_3Sb_4$-57207; $Cu_3Nd_3Sb_4$-658635; $Cu_3O_2Ru_4Sr$-51895; Cu_3O_6Te-1529; Cu_3O_6Te-26990; $Cu_3Pr_3Sb_4$-658639; Cu_3S_3Sb-31113; $Cu_3Sb_4Tb_3$-658642; $Cu_3Sb_4U_3$-657096; $Cu_3Sb_4Y_3$-658636; $Cu_3Sn_4U_3$-629298; Cu_5Zn_8-2092; $Dy_2Fe_{32}O_2$-9639; Dy_2O_3-66736; $Dy_3Fe_5O_2$-23856; $Dy_3Ga_5O_2$-409391; Dy_3S_4-630201; Dy_3Se_4-630252; Dy_4Ga_2Ni-629724; $Dy_4Ni_2Sn_{25}$-160045; Dy_4Sb_3-630245; ErF_3-81411; Er_2O_3-39521; Er_3F_0K-418210; Er_4Sb_3-600631; EuF_2-29025; $EuFe_4P_2$-79925; $EuNa_0Sn_2$-172209; $EuRu_4Sb_2$-79928; Eu_3F_0Rb-14027; $Eu_3Ga_4Ni_4$-103395; Eu_3S_4-100522; F_0KTb_3-28214; F_0KY_3-155137; F_0KYb_3-28258; $F_2Fe_2Li_3Na_3$-17056; F_2KTb_3-51125; F_2P_4Pt-418726; F_3KSb_4-24740; F_3KSb_4-4049; F_4N_2Ni-26397; F_5Nb_6-25769; FK-53824; FK-61558; FLi-184904; FLi-62361; FMg_2N-262328; FNa-262837; FRb-43436; FRb-53828; FSeY-1827; FTl-16112; FTl-16113; FTl-28495; FTl-30268; FTl-90993; FTl-90994; FTl-9873; F_2Fe-14143; F_2Ge-18030; F_2HK-9345; F_2HRb-45859; F_2Hg-33614; F_2Hg_2-23719; F_2Hg_2-27700; $F_2Hg_3S_2$-16927; F_2Kr-23534; F_2Kr-279623; F_2Mg-422263; F_2Mg-51242; F_2Mg-51243; F_2Mg-56506; F_2Mg-94284; F_2Mn-12167; F_2Mn-200641; F_2Mn-20365; F_2Ni-26605; F_2Ni-34307; F_2Pb-161391; F_2Pb-60014; F_2Pd-100567;

F_2Pd-16763; F_2Sn-14194; F_2Sn-14195; F_2Sn-308; F_2Sr-168801; F_2Sr-41402; F_2Ti-68400; F_2V-201245; F_2Xe-28334; F_2Zn-184219; F_3Fe-202047; F_3Fe-240398; F_3Fe-52167; F_3FeK-44784; F_3FeRb-49586; F_3Ga-22197; F_3HgRb-15169; F_3Ho-200955; F_3I-411036; F_3In-18028; F_3Ir-77619; F_3KMg-40476; F_3KMn-246919; F_3KMn-246921; F_3KMn-43721; F_3KMn-75412; F_3KMn-75414; F_3KNi-15426; F_3KPd-73167; F_3KV-28145; F_3KZn-56097; F_3La-164054; F_3La-164055; F_3La-167553; F_3La-16964; F_3La-246323; F_3La-27089; F_3La-28538; F_3La-3; F_3La-34108; F_3La-96133; F_3La-96134; F_3MgNa-171813; F_3MgRb-49585; F_3Mg_3N-18320; F_3MnRb-43722; F_3Mo-30612; F_3Mo-68527; F_3NaV-60611; F_3Nb-25596; F_3Nd-16967; F_3Nd-63049; F_3Nd-63050; F_3Ni-87943; F_3PbRb-49591; F_3Pd-16675; F_3Pr-16966; F_3Pu-29013; F_3RbV-28146; F_3RbYb-49590; F_3Rh-29134; F_3Ru-16673; F_3Sb-30411; F_3Sc-261067; F_3Sc-30215; F_3Ta-30613; F_3Tb-167474; F_3Ti-52162; F_3Tl-10365; F_3U-24966; F_3V-30624; F_3Y-15961; F_3Y-6023; F_3Yb-9844; F_4Ge-202558; F_4Hf-66008; F_4HgRb_2-72352; F_4Ir-23483; F_4K_2Mn-23184 (33); F_4K_2Ni-73450 (55); F_4K_2Zn-100298 (98); F_4LiLu-152948; F_4LiSc-413966; F_4LiY-39563; F_4LiY-55692; F_4LiYb-9914 (6); F_4MgRb_2-69681 (6); F_4Nb-23949; F_4Pb-16795; F_4PbPd-108992; F_4Pd-1555; F_4PdSr-108990; F_4Pt-71579; $F_4S_2Yb_3$-92497; F_4Se-85451; F_4Si-14122; F_4Si-63184; F_4Sn-16794; F_4SrZn-31367; F_4Te-9869; F_4V-65785; F_4Xe-27467; F_4Zr-35100; F_5H_8N-38338; F_5I-6021; F_5Mo-26644; F_5Nb-26647; F_5P-62554; F_5U-200459; F_5U-31658; F_6FeZr-100301 (48); F_6FeZr-35716 (90); F_6GeRb_2-68982 (27); F_6HfK_2-47244; F_6HfV-94455; F_6KP-25576; F_6K_2Mn-47213; F_6K_2Ni-41416; F_6K_2Si-73722; F_6K_3Mo-4403; F_6K_3W-51264; F_6LiNb-165202; F_6LiP-74830; F_6LiSb-23924; F_6Li_2Zr-409667; F_6MnRb_2-47207; F_6Mo-153; F_6Mo-1879; F_6MoNa-31033; F_6NaP-90615; F_6NaSb-25538; F_6NaSb-56251; F_6NiRb_2-29005; F_6O_2Pt-28345; F_6O_2Sb-78849; F_6PTl-28899; F_6Pb_2-23467; F_6PdRb_2-28675; F_6Rb_2Si-38547; F_6Rb_3Tl-19075; F_6Rb_3Y-19077; F_6S-214; F_6S-41229; F_6S-63360; F_6S-63362; F_6SiTl_2-38549; F_6SiTl_2-52292; F_6Sn_2-33786; F_6Te-67609; F_6TiTl_3-42154; F_6TiZr-94456; F_6U-2499; F_6VZr-94454; F_6W-4027; F_6Xe_2-18128; F_7I-31691; F_7IXe-26059; $F_7K_3Mn_2$-33525; $F_7K_3Ni_2$-33523; $F_7K_3Zn_2$-100299; F_7Li_3Th-1726; F_7Re-78311; F_8Na_2U-165293; F_8Na_3Pa-16153; F_8Sn_3-32592; F_9U_2-35288; $FeGa_6Ge_6Tb_4$-281082; $Fe_2Ge_3Mn_3O_2$-18111; $Fe_2Mg_3O_2Si_3$-27373; $Fe_{32}Ho_2O_2$-9827; $Fe_{32}O_2Y_2$-9640; $Fe_3Mn_2O_2Si_3$-27378; $Fe_3O_2Si_3V_2$-27376; Fe_4LaP_2-1286; Fe_4LaSb_2-53490; Fe_4NdP_2-93364; Fe_4NdSb_2-79927; Fe_4P_2Pr-93363; Fe_4P_2Tb-245293; Fe_4P_2Th-200827; Fe_4P_2U-633114; Fe_4P_2Yb-156464; $Fe_5O_2Si_3$-27377; $Fe_5O_2Tb_3$-9233; $Fe_5O_2Y_3$-29235; $Fe_5O_2Yb_3$-23854; Fe_5Si_3-161132; Ga_2PdTb_4-153210; Ga_2PdY_4-103910; Ga_2PtTb_4-153211; Ga_2PtY_4-153909; GaI_3La_3-409561; $GaLi_3N_2$-25566; $GaLi_5O_4$-16926; $Ga_3Na_3O_2Te_2$-418645; Ga_4Mn-634630; $Ga_5Ho_3O_2$-409390; $Ga_5O_2Tb_3$-20831; $Ga_5O_2Y_3$-23852; $Ga_5O_2Yb_3$-23851; Ga_7Ni_3-408313; Gd-104045; $GdLiO_2$-422561; Gd_2O_3-40473; Gd_3I_3Si-67361; $Gd_3Ni_6Si_2$-601071; $Gd_3O_2Sb_5$-65147; Gd_3S_4-636328; Gd_3Se_4-636389; Gd_4Sb_3-601400; Ge-181072; GeI_3La_3-414174; $GeLi_2O_5Ti$-250297; Ge_3La_4-76313; Ge_3N_4-97569; Ge_4Li_5-43235; $Ge_6Ir_7Mn_4$-153070; $Ge_6Ir_7Yb_4$-413984; $Ge_6Lu_4Rh_7$-90200; $Ge_6Lu_4Ru_7$-90199; $Ge_6Os_7Sc_4$-637471; $Ge_6Rh_7Sc_4$-84201; $Ge_6Rh_7Yb_4$-413983; Ge_7Ir_3-53656; $Ge_8Na_6Pt_8$-32038; H_5Th_4-24686; H_4Li_2Mg-181325; Hf_3N_4-97997; Hg_3O_6Te-30325; Hg_4Ni-639118; Hg_4Pt-659824; Ho_2O_3-27773; Ho_4Sb_3-601431; $ILiO_3$-20032; $ILiO_3$-40363; I_3La_3P-411801; I_3La_3Pb-409796; I_3La_3Sb-411804; In_2O_3-14387; In_7Pd_3-408314; In_7Pt_3-59500; K_0Pb_{48}-410090; $K_2O_3Sn_2$-40463; K_3S_4Sb-41895; $K_8O_{24}Sr_2U_6$-91784; LaP_2Ru_4-50596; La_2O_3-96201; La_3S_4-56782; La_3Se_4-60208; La_3Te_4-642013; $La_4O_9Re_6$-22207; $La_4O_9Re_6$-36083; $La_4O_9Ru_6$-100098; La_4Pb_3-641648; La_4Rh_3-641734; La_4Sb_3-10441;

$La_6P_7Pd_6$-30850; $Li_2Mg_3Si_4$-39596; Li_5Si_4-159397; LiN_2P-66007; Li_2O_3Si-100402; Li_2O_4S-153807; Li_2O_4S-58; Li_2O_4W-10479; Li_2O_4W-15395; $Li_2O_5Si_2$-78562; Li_3NbO_4-30246; $Li_3Nd_3O_2W_2$-245640; Li_3O_4P-10257; Li_3O_4P-20208; Li_3O_4Ta-37126; Li_3O_4V-19002; Li_4O_4Ti-75164; Li_6O_4Zn-62137; $Li_6O_7Si_2$-25752; $Li_6O_7Zr_2$-41321; Li_7O_6Ta-74950; Lu_2O_3-33659; $Mg_3Mn_2O_2Si_3$-27374; Mg_3N_2-23522; $Mg_3O_2Si_3V_2$-27372; Mg_3P_2-26875; Mg_3Sb_2-181285; $Mg_4P_6Rh_7$-94390; Mn_2O_3-9091; $Mn_3O_2Si_3V_2$-27380; $Mn_5O_2Si_3$-27382; Mn_7NaO_2-19022; Mo_3Sb_7-24303; $N_2P_6SZn_4$-76440; $N_{24}O_2P_2Zn_8$-417324; N_2O_4-29047; N_2Zn_3-84918; N_3U_2-644812; N_4Si_3-97567; N_4Zr_3-97998; Na_0Sn_2Sr-240007; Na_0Sn_2Yb-172210; Na_3O_3Sb-23346; Na_3S_4Sb-44707; Na_3SbSe_4-65141; Na_6O_4Pb-21059; NbS_4Tl_3-600246; $NbSe_4Tl_3$-600249; $Nb_3Sb_2Te_5$-417101; $NdOs_4Sb_2$-79929; Nd_3S_4-645823; $Nd_4O_9Os_6$-200870; Nd_4Sb_3-645890; NiP_3-23714; $Ni_3Pb_2S_2$-159363; $Ni_3Sb_4U_3$-23078; $Ni_3Sb_4Zr_3$-87995; $Ni_3Sn_4Th_3$-657422; $Ni_3Sn_4U_3$-105374; $Ni_3Sn_4U_3$-646805; Ni_6PbY_2-54614; $O_2Pr_3Sb_5$-22502; $O_2Sb_5Yb_3$-20945; OTa_2-28387; $O_{36}P_2Sc_4$-1719; O_3V_2-260212; O_4Pt_3-27836; O_6Rb_4-25718; O_6Sr_2WZn-28599; O_8SnTe_3-9077; O_8Te_3Ti-9076; O_8Te_3Zr-9079; Os_3Sn_7-54605; Os_4PrSb_2-155178; P_2Ru_4Tb-245294; P_3Rh-23712; P_3Ti_4-648219; P_4Th_3-25724; P_4U_3-25725; Pb-54314; $Pb_2Pd_3S_2$-159365; Pd_6S_7-32053; $Pr_3Pt_3Sb_4$-649207; Pr_3S_4-649249; Pr_3Se_4-649323; Pr_3Te_4-649411; Pr_4Sb_3-649308; $Pt_3Sn_4U_3$-649697; $Re_7Si_6U_4$-2471; $RhSb_3$-34049; $Rh_7Sb_6Yb_4$-409885; $Rh_7Sb_6Yb_4$-421488; Ru_3Sn_7-54510; Ru_4Sb_2Sr-42962; S_3Tm_2-39240; S_3Yb_2-72010; S_4Sm_3-2245; S_4TaTl_3-16571; S_4Tl_3V-16572; S_4Tl_3V-600245; Sb-108182; Sb_3Tb_4-601429; Sb_3Yb_4-43031; Sb_3Yb_4-651757; Sb_4Th_3-16655; Se-104187; Se_4Sm_3-651872; Se_4TaTl_3-52431; Se_4Tb_3-651982; Se_4Tl_3V-600248; Se_4U_3-23710; SiV_3-52472; Sm_3Te_4-652658

Reference

1. Gong, W.; Tabata, T.; Takei, K.; Morihama, M.; Maeda, T.; Wada, T. Crystallographic and Optical Properties of (Cu, $Ag)_2ZnSnS_4$ and (Cu, $Ag)_2ZnSnSe_4$ Solid Solutions. Phys. Status Solidi C **2015**, 12, 700−703.